Double-Ducted Fan as an Effective Lip Separation Control Concept for Vertical-Takeoff-and-Landing Vehicles

Ali Akturk* and Cengiz Camci†
The Pennsylvania State University, University Park, Pennsylvania 16802

This paper describes a novel inlet flow conditioning concept that significantly improves ducted fans' performance and controllability. High angle-of-attack operation of ducted fans is very common in vertical-takeoff-and-landing systems. The new concept named double-ducted fan (DDF) uses a secondary shroud to control inlet lip-separation-related momentum deficit at the inlet of the fan rotor during edgewise flight. The DDF is helpful in a wide edgewise flight velocity range, and its corrective aerodynamic effect becomes more pronounced with increasing flight velocity. A conventional baseline duct operating at 90 deg angle of attack is compared to other novel double-ducted fan designs via three-dimensional, viscous, and turbulent flow computations. A custom actuator-disk model replaces the zonal computation of the complex and three-dimensional rotor flowfield in the rotating frame of reference. Both hover and edgewise flight conditions are considered around the ducted fan unit and inside the ducts. Significant improvements from several novel ducted fan designs are in the areas of vertical thrust enhancement, nose-up pitching moment reduction, and recovery of fan through-flow mass flow rate in a wide horizontal flight range. A variable DDF design, a partial DDF design, and a fan-in-wing implementation of the DDF are introduced.

Nomenclature

β_1	=	blade section inlet angle, deg
β_2	=	blade section exit angle, deg
c	=	chord length, m
c_1	=	rotor inlet absolute velocity, m/s
c_2	=	rotor exit absolute velocity, m/s
c_θ	=	tangential (swirl) component of the velocity, m/s
c_x	=	axial component of the velocity, m/s
D	=	overall tip diameter of the baseline ducted fan, m
e	=	internal energy, which is equal to $c_v.T$
h	=	rotor blade height, $r_{tip} - r_{hub}$
p	=	static pressure, Pa
r	=	radial distance measured from the origin, m
t	=	rotor tip clearance, m
w_1	=	rotor inlet relative velocity, m/s
w_2	=	rotor exit relative velocity, m/s
X	=	axial distance measured from the inlet plane of the standard duct, m
x	=	X/c, nondimensional axial distance
α	=	angle of attack, deg
ρ	=	density, kg/m^3
Ω	=	rotational speed, radian/s

I. Introduction

DUCTED-FAN-TYPE propulsion offers an attractive solution by providing operational safety and compact vehicle/payload packaging. Ducted fans offer a higher thrust-to-power ratio than free rotors due to the propeller jet stream's diffusion. When a vertical takeoff and landing (VTOL) ducted fan is in edgewise flight, the relative inlet flow is "normal" to its axis of rotation. Severe problems related to flow separation at the leading edge of the duct lip are encountered. This angle between the axis of rotation and inlet flow direction is usually termed "angle of attack." At a high angle of attack, the inlet flow separation leads to aeromechanical problems within the duct. It may result in a high nose-up pitching moment and severe recirculatory flow patterns. High levels of local turbulence, mechanical vibrations, and noise are encountered as the edgewise flight speed increases. Therefore, measuring and predicting ducted fans' mean flow characteristics are crucial to understanding the problems related to reliable and controllable horizontal flights of VTOL vehicles.

A. Early Ducted Fan Studies

Numerous studies were undertaken to quantify and improve the flowfield characteristics around ducted fans. The power requirement of a ducted fan is less than a propeller of the same diameter in isolation for equivalent static thrust. McCormick [1] explained the reduced power demand because of the thrust produced by the duct and the reduction in tip losses occurring between the fan rotor and the casing. The pressures on the duct surface created by the flow induced by the fan contribute to the overall forces and moments acting on the vehicle. In an earlier study, Lazareff [2] reported that a shrouded propeller is not merely a free propeller with a shroud around it. He explained the interest raised by this system by its capability to ensure a hovering flight with fuel consumption and noise levels very much less than that of a turbojet. He also predicted a forward subsonic flight higher than that of a free propeller. An experimental investigation has been one of the major approaches to study the flow characteristics of ducted fans. Abrego and Bulaga [3] performed wind-tunnel tests to determine ducted fans' performance characteristics for axial and edgewise flight conditions. Martin and Tung tested a ducted fan VTOL UAV (uninhabited aerial vehicle) with a 10-in.-diameter fan rotor [4]. They measured aerodynamic loads acting on the vehicle for various angles of attack in hover for different crosswind velocities. They also included hot wire velocity surveys at the duct's inner and outer surface and across the downstream wake. The authors emphasized the influence of the tip gap height on the thrust force produced. They underlined the importance of tip vortex and duct boundary-layer interaction. Their study also showed the effect of the duct's leading-edge radius on the fan system's stall performance and stability. Graf et al. [5,6] improved ducted fan edgewise flight performance using a newly designed leading-edge geometry. They determined that leading-edge geometry is a significant factor in offsetting adverse aerodynamic characteristics. Kriebel and Mendenhall also carried out a theoretical and experimental study to predict ducted fan performance [7]. They developed methods for predicting the forces and moments on the duct, duct surface pressure distributions, and boundary-layer separation. They compared their predictions with

*Professor of Aerospace Engineering, Turbomachinery Aero-Heat Transfer Laboratory, Department of Aerospace Engineering. Member AIAA.
†Turbomachinery Aero-Heat Transfer Laboratory, Department of Aerospace Engineering; currently Principal Engineer, Siemens Energy, Orlando, FL. Member AIAA.

measurements made on Bell X-22A and Doak VZ-4 aircraft models. Their model qualitatively predicted the force and moment, the pressure distribution, and the separation of the boundary layer over the entire operating range of propeller thrust and angle of attack. Mort and Gamse [8] investigated the aerodynamic characteristics of a 7-ft-diameter ducted propeller used on Bell Aerosystems Company's X-22A airplane. They reported aerodynamic characteristics for power variations, freestream velocity, blade angle, and duct angle of attack. The stall of both the upstream and downstream duct lips of this 7-ft-diameter ducted fan was examined as a function of angle of attack. Mort and Yaggy [9,10] performed hover and edgewise flight tests on a 4-ft-diameter wing-tip mounted ducted fan used on Doak VZ-4-DA. They emphasized that the pitching moment rapidly changed, and the required power increased due to inlet flow separation, which occurred near the windward side duct lip. They also reported that a ducted fan supported by a fixed wing required less power than a free-flying ducted fan.

B. Computational Efforts for Ducted Fans

In addition to experimental studies, the ducted fan design and performance analyses benefitted from computational flow modeling. Lind et al. [11] carried out a computational study using a panel method. They compared their results to the experimental results from Martin and Tung [4]. He and Xin [12] developed their ducted fan models based on a nonuniform and unsteady ring vortex formulation. Chang and Rajagopalan [13] developed a grid generation methodology known as "the curve adaptive option" to model several industrial ducted fans. An incompressible Navier–Stokes solver was implemented to calculate the flowfield of a duct fan. The computational results agreed well with available wind-tunnel data. Ahn and Lee [14] applied a computational method to their ducted fan system to identify the design parameters that affect its performance. Ko et al. [15] developed a computer code to design a ducted fan system. Zhao and Bil [16] proposed a computational fluid dynamics (CFD) simulation to design and analyze an aerodynamic model of a ducted fan UAV in the preliminary design phase with different speeds and angles of attack. Ohanian et al. [17] investigated the challenging problem of representing a ducted fan configuration in terms of traditional nondimensional coefficients. Their effective analysis of wind-tunnel data for a generic ducted fan configuration led to a unique nondimensional modeling scheme. They presented a new wind-tunnel correction scheme for ducted fans and a new statistical modeling technique that attained a very high correlation for present and legacy data. They were able to represent ducted-fan aerodynamics using 12 nondimensional coefficients.

C. Synthetic Jets and Controllability of Ducted Fans

"Ducted-Fan Force and Moment Control via Steady and Synthetic Jets" for leading- and trailing- edge flow control was introduced by Ohanian, et al. [18]. The flow-controlling piezoelectric synthetic jets were actuated asymmetrically around the circumference to produce control forces and moments. The synthetic and steady jets both produced noticeable effects in the duct trailing-edge. However, from a practical standpoint, the ducted-fan implementation required more flow control authority than the synthetic jets could deliver. Synthetic jets were useful in inducing duct leading-edge separation comparable with that obtained from steady jets running at blowing rates that were an order of magnitude higher than those of the piezoelectric synthetic jets. Leading-edge separation on the duct lip was induced at high angles of attack through synthetic and steady jet blowing, which also decreased pitching moment. "Control System Effectiveness for [small military] Ducted Fan VTOL UAVs Operating in Crosswinds" was investigated by Fleming et al. [19]. A critical operational problem of ducted-fan-based vehicles is their precise control under crosswinds and turbulent conditions. The authors claim that "there are two significant, inherent issues associated with ducted fan control in crosswinds; 1) lateral momentum drag and 2) a duct stabilizing torque which [sic] resists tipping into the wind." Control in the longitudinal plane was the research focus, and most wind-tunnel results were obtained with the vehicle in a hover orientation. Their

experimental study used a 10-in-internal-diameter ducted fan with a 19% thick airfoil-shaped duct cross section. Four flapped control vanes were positioned at about 1 duct diameter aft of the duct quarter chord. They also used a simplified computational fluid dynamics (CFD) modeling approach during this project to support their wind-tunnel findings. Several auxiliary control concepts were analyzed, and wind-tunnel tested to improve the controllability of VTOL UAVs in a crosswind. They showed that these devices could be helpful when used in conjunction with the primary control vanes, as more significant pitching moment could be obtained with relatively simple control components. At high forward speeds, the edgewise flight will significantly increase the pressure drag of the duct facing the oncoming wind. UAVs would likely use some form of mechanism to rotate the ducted fans to function as propulsors. Thus, the lip separation would be of concern during transitional flight as the vehicle transitions from vertical hover to forward flight.

D. Blade Tip Vortices, Flow Reversal Behind Rotor, and Wake Vortex

A RANS-based CFD analysis of ducted-fan flow was the topic of investigation in [20], Ruzicka et al. The application of overset grid methods to studying the flowfield of the FANTAIL™ antitorque system of the RAH-66 rotorcraft was under investigation. In addition to a wind-tunnel experimental program, flowfield visualizations were presented and used to explain how the blade tip vortices combined with the adverse pressure gradient beneath the rotor disk to impact flow along the duct wall. The study showed that proper grid refinement in the vicinity of the blade–shroud gap was crucial in obtaining a converged solution and resolving key flow details within the gap. The thrust-power predictions showed good agreement with the experiment, and the CFD-based visualizations demonstrated that reverse flow under the rotor is the result of blade tip vortices rather than duct divergence. Gray and Wright [21] mentioned that, like a free aircraft propeller, a ducted fan generates a wake vortex system originating from the rotor airfoil trailing edges whose motion is that of helical surfaces. A mathematical model of the constant-diameter vortex wake was developed for zero hub diameter and neglected compressibility, viscosity, and tip clearance. They found that the numerical procedures employed for replacing the vortex system of a ducted fan with several finite-strength vortex filaments were satisfactory. Wright [22] developed a mathematical model for the vortex wake system of a heavily loaded ducted fan for zero hub diameter, neglecting compressibility, viscosity, and tip clearance. He showed that the blade vortex strength distribution for the heavily loaded ducted fan could be extracted from the lightly loaded case using a simple scaling factor for any blade number and pitch angle choice. A CFD study of an annular-ducted-fan-based lift system for VTOL aircraft was conducted by Jiang et al. [23]. The power and lift efficiency of the lift fan in hover mode, the lift and drag in transition mode, the drag and flight speed of the aircraft in cruise mode, and the pneumatic coupling of the tip turbine and jet exhaust were studied. The CFD simulation indicated that the annular-ducted-fan system has higher lift efficiency than the rotor of a helicopter due to the additional duct lift and the elimination of energy losses. The transition from hover to cruise flight requires extra forward thrust to overcome a low peak of drag, primarily caused by the momentum drag of the low disk loading fan system.

E. Fan-in-Wing Studies

Fan-in-wing (FIW) aircraft, distinct from existing air vehicles, use a fixed wing with a forced airflow produced by ducted fans mounted inside the wing. FIW aircraft received renewed interest in the naval community using VTOL aircraft to support naval operations. Sheng and Zhao [24] investigated the aerodynamic performance of a fan-in-wing configuration in hover. They numerically investigated FIW aerodynamics using a high-fidelity three-dimensional unsteady Reynolds-averaged Navier–Stokes flow solver based on unstructured grid technology. They introduced an active flow control concept to enhance the VTOL vehicle's operating efficiency and thrust level by increasing the fan-in-wing configuration's circulation and duct mass

flow rate. Numerical predictions for this active control concept showed a 25%–55% increase in the maximum thrust, achieved without suffering the peak efficiency loss. Hoeveler et al. [25] investigated the aerodynamic behavior of a nonrotating lifting fan remaining uncovered during cruise flight instead of being covered by a shutter system. They focused on the additional drag and loss of lift of an uncovered fan-in-wing. In a wind-tunnel study of a wing-embedded lift fan using force, pressure, and stereoscopic particle image velocimetry, they showed that a step on the lower side of the wing in front of the lifting fan duct increases the lift-to-drag ratio up to 25% for all positive angles of attack. A doubling of the curvature radius of the lifting fan duct inlet lip on the upper side affected the lift-to-drag ratio by less than 1%. They concluded that the lifting fan duct inlet curvature could be optimized to maximize the vertical fan thrust of the rotating lifting fan during hover without affecting the cruise flight performance with a nonrotating fan.

F.   Influence of Duct Shape and Inlet Geometry

An experimental study of the performance of a ducted propeller designed for UAV applications at zero-angle-of-attack flight was presented by Yılmaz et al. [26]. They used five different duct shapes under hover and forward flight conditions. Experiments conducted in a subsonic wind tunnel showed that the power coefficients obtained for all ducted propeller arrangements were less than that of the open propeller, which indicates that the propeller operates more efficiently inside a duct. However, thrust obtained from the duct decreased and reached negative values with increasing advance ratio, which made the duct unfavorable at high freestream velocities. Pressure measurements showed that the origin of the duct thrust is the suction effect induced by the propeller in the converging part of the duct. Optimization of inlet shape for all advance ratio range of the vehicle was essential for a better design. Werle [27] developed a simple, accurate, reduced-order model for predicting the maximum available thrust of subsonic ring-wing propulsors varying in shroud airfoil length, thickness, camber, and angle of attack relative to the centerline. The method applies to drones, aircraft, and ships. The model's accuracy was assessed using more than 40 published experimental and computational data sets for more than 20 different configurations. Werle showed that the model's algebraic solutions provide outstanding engineering estimates under all operating conditions from hover to cruise, enabling a rapid preliminary design of ring-wing-based systems. The new model also provided a valuable point of departure for initiating more complex design optimization, including the integrated shroud and propeller design.

G.   Past Work Leading to DDF Concept Development

The authors of this paper [28] experimentally studied the inlet flow distortion of a vertical and short take-off and landing (V/STOL) ducted fan in hover and forward flight regimes. They used a planar particle image velocimeter (PIV) to investigate the near duct aerodynamic performance. The aerodynamic modifications due to fan inlet flow distortions in the forward flight regime were visualized and documented in the PIV results. A radial equilibrium-based fan aerodynamic model combined with angular momentum conservation principle and energy equation was effectively integrated into a three-dimensional (3-D) RANS-based computational system. PIV measurements and time-efficient computational predictions of the mean flow near the fan inlet plane were in very good agreement under hover conditions. Akturk and Camci [29] gave a detailed description of the actuator-disk model replacing the rotor flow for the current 3-D RANS computations for the time efficiency of 3-D viscous flow computations. Akturk and Camci explained a comprehensive validation effort of the RANS-based CFD model used in this study [30,31]. They focused on the grid generation features, the grid sensitivity results, the turbulence model, and experimental validation cases for the current double-ducted-fan (DDF) computations. Camci et al. [32] also discussed the aerodynamic impact of tip clearance and inlet flow separation control ability of lip-spoilers for VTOL UAVs.

This paper aims to improve ducted fan flow characteristics by developing a novel inlet flow control and conditioning concept. This unique aerodynamic approach significantly enhances the aerodynamic performance and controllability of VTOL vehicles and many other ducted-fan-based systems. The new idea that reduces the inlet lip separation-related performance penalties in the edgewise flight zone is named "double-ducted fan *(DDF)*." The current concept uses a secondary stationary duct to control and reduce *inlet lip separation*, occurring at elevated edgewise flight velocities and high angles of attack. The DDF self-adjusts in a wide edgewise flight velocity range regarding its lip-separation-related passive flow control ability.

A preliminary and brief account of the DDF concept developed by the authors was also presented as an American Society of Mechanical Engineers (ASME) conference paper [33] and some of the results discussed in [33] are included here with permission from the ASME. The DDF as a novel concept was also explained in a current U.S. patent by Camci and Akturk [34].

II.   Upstream Lip Region Flow and Adverse Effects of Lip Separation in Edgewise Flight

Ducted fan systems in edgewise flight all inherently have an inlet flow direction that significantly deviates from the axis of the rotation of the fan. A 90 deg angle of attack is typical. The inlet flow distortion near the leading side of all of these fans becomes more problematic with increasing vehicle speed. The flow separation occurring on the lip section's inner side severely limits VTOL UAVs' lift generation and controllability. In general, the fan's leading side near the lip separation zone breathes poorly compared to the trailing side. The trailing side's total pressure is usually much higher than that of the leading side at the rotor's exit. A separated flow zone near the leading side adversely affects the flow, causing a highly recirculatory, low-momentum, unsteady, and turbulent flow system. Severe mechanical vibrations originating from this region are typical.

Conventional ducted fan systems also have a tip clearance loss proportional to the effective tip gap size. The tip region's specific shape and the surface properties and arrangements designed onto the casing inner surface also influence the magnitude of tip clearance loss. This aerodynamic deficiency is a significant total pressure loss near the tip at the rotor's exit when the vehicle is only hovering with no horizontal flight. When the vehicle transits into an edgewise flight, the total pressure loss at the exit of the rotor near the leading side is much more significant than "hover only" loss. This transition is an off-design condition for an axial flow fan that is usually designed for a reasonably uniform inlet "axial" velocity profile in the rotor's spanwise direction. The immediate impact of any inlet flow distortion entering into an axial fan rotor in edgewise flight are the loss of rotor's energy addition capability to the fluid near the leading side, an imbalance of the local mass flow rate between the leading side and trailing side, and an imbalance of the total pressure observed at the rotor exit between the leading side and trailing side. A significant loss of lifting ability due to highly nonaxisymmetric and unnecessarily 3-D fan exit flow occurs. An unwanted nose-up pitching moment generation because of the local static pressure distributions imposed on the inner duct surfaces is typical for this common off-design operation at a high angle of attack. The body-axis coordinate system, pitching moment, and lift-and-drag forces acting on a ducted-fan-based UAV system operating at a high angle of attack is shown in Fig. 1, Graf [6].

At a high angle of attack, the onset of separation at the upstream duct lip is accompanied by a separation bubble. The existence of a significant separation bubble severely distorts the inlet flow of the fan rotor, especially near the leading side and in the tip clearance region. Distorted inlet flow causes an asymmetric loading of the ducted fan, which increases the power required for level unaccelerated flight. The immediate results of operating a ducted fan in a horizontal flight regime, especially at a high angle of attack, are as follows:

1. Increased aerodynamic losses and temporal instability of the fan rotor flow occurs when "inlet flow distortion" from "the lip separation area" finds its way into the tip clearance gap, resulting in the loss of "energy addition capability" of the rotor.
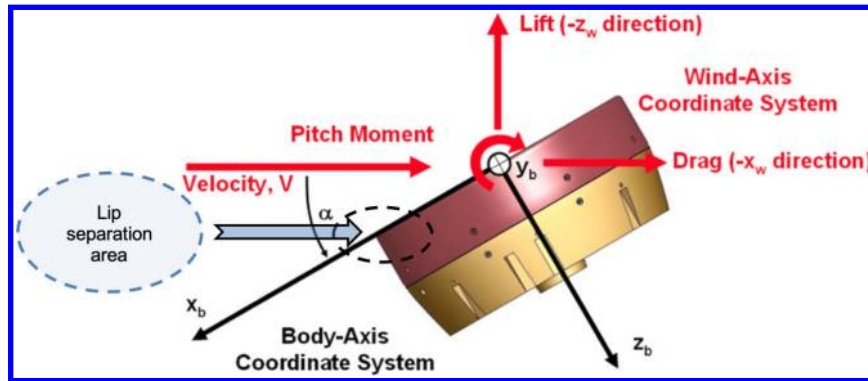
Fig. 1 High angle-of-attack operation of a ducted-fan-based UAV, body-axis coordinate system, pitching moment, and lift and drag, from Graf [6].

2. Reduced thrust generation is due to the rotor breathing low-momentum, recirculatory, turbulent flow from the duct's upstream side.

3. A severe imbalance of the duct "inner casing" static pressure field results from low-momentum fluid entering into the rotor on the leading side, and high momentum fluid is unnecessarily energized near the rotor's trailing side.

4. There is a measurable increase in power demand and fuel consumption when the lip separation occurs to keep up with a given operational task.

5. Lip separation and its interaction with the tip gap flow require a more sophisticated vehicle control system because of the exit jet's severe nonuniformity in the circumferential direction and excessive nose-up pitching moment generation.

6. A severe limitation in the rate of descent and vehicle controllability may occur at low horizontal speeds because of more pronounced lip separation. Low power requirement of a typical descent results in a lower disk-loading and more pronounced lip separation.

7. Complex unsteady interactions of duct exit flow occur with control surfaces.

8. Excessive noise and vibration occur because of the rotor working with a significant inlet flow distortion.

A. Lip Separation at High Angle of Attack

Previous research results demonstrating the limits of onset of upstream lip separation in function of angle of attack are summarized in Fig. 2. A full-scale duplicate of the V/S TOL ducted propeller used on the Bell Aerosystems Co. X-22-A airplane was tested in Ames Research Center by Mort and Gamse [8]. The stall of both the upstream and downstream duct lips of this 7-ft-diameter ducted fan was examined in function of angle of attack. The angle of attack of the ducted fan is measured between the approaching flow direction and the axis of rotation of the rotor. It was found that the onset of separation on the upstream lip would be encountered; however, complete separation on this lip would be encountered only during
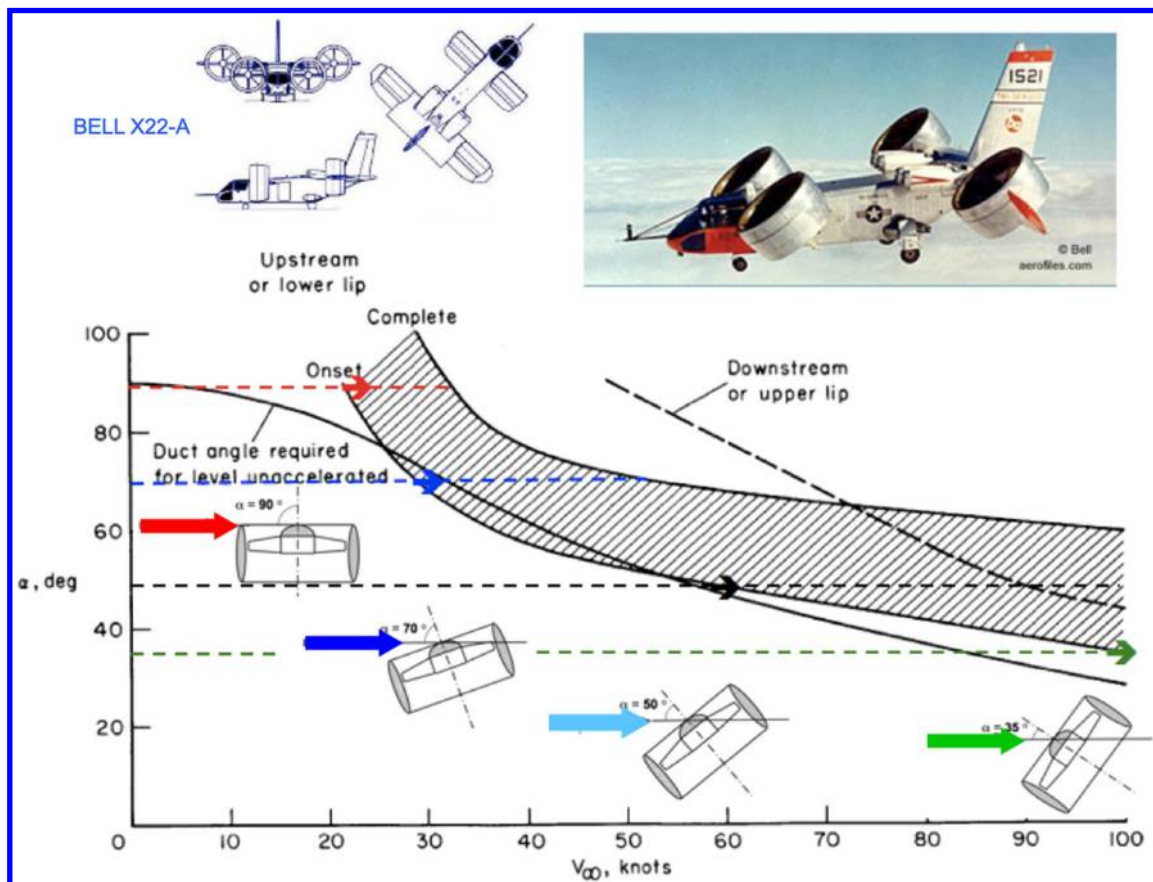

Fig. 2 Limits of onset of upstream lip separation in function of angle of attack, from Mort and Gamse [8].

conditions of low power and high duct angle of attack corresponding to high rates of descent.

III. Double-Ducted-Fan Concept, Research Hypothesis, and Objectives

The investigation started with nine different configurations, which differ in channel size, second duct height, channel minimum width, and configuration weight. The final two configurations were chosen based on the following criteria: inlet lip separated-reduction drag reduction, weight reduction, vehicle pitching moment reduction, and thrust increase. The configurations that were not effective in separation control were not included for brevity. Figure 3 shows the new ducted fan inlet-flow-control concept called "DDF" as a significant improvement over a standard ducted fan. The streamline patterns and the velocity magnitudes in a vertical plane passing from the leading edge and trailing edge of the baseline fan are presented.

The poor edgewise flight characteristics of the reference duct, as shown in Fig. 3a, are effectively improved with the double-ducted-fan concept, illustrated in Fig. 3b. A typical deficiency of a standard ducted fan is mainly related to the forward lip separation increasingly occurring when the edgewise flight velocity is gradually increased, as shown in the streamline patterns of Fig. 3a. Figure 3b shows the reduced lip separation obtained by implementing DDF at 20 m/s forward flight speed.

The inlet flow near the leading side of the standard duct is highly separated, low-momentum, and turbulent. The apparent flow imbalance between the leading and trailing sides of the standard ducted fan, as shown in Fig. 3a, causes an inlet flow distortion. Figure 3a indicates that the rotor barely breathes at the leading-side inlet section, although the trailing side passes a significant amount of flow. This flow imbalance amplified during the rotor "energy adding process" is one of the reasons for substantial nose-up pitching moment generation. Figure 3b also presents the double-ducted-fan (DDF) flow simulations, indicating the effective inlet flow distortion reduction due to the new (DDF) system's unique aerodynamic properties. The upstream lip separation near the leading side is almost eliminated, resulting in a more balanced rotor exit flowfield between the leading side and the trailing side.

A. Geometric Definition of a Typical DDF Arrangement

The DDF concept benefits from a second duct using an airfoil shape with a relatively shorter axial chord length than that of the standard duct. The critical parameter in obtaining an effective DDF arrangement is the lip diameter DL of the standard ducted fan. The airfoil used for the second duct is slightly cambered and has a leading-edge diameter set to 0.66 DL, as explained in Fig. 4b. The second duct airfoil's angular orientation and axial position are critical in achieving an adequate flow improvement near the leading side of the rotor. The second duct airfoil's leading-edge circle is slightly shifted in the vertical direction for proper inlet lip separation control. The vertical distance between the duct inlet plane touching the standard duct and the plane touching the second duct is about 0.33 DL, as shown in Fig. 4b. The horizontal distance between the centers of the leading-edge circles of the standard duct and outer duct is about 4 DL. The axial chord of the second duct airfoil is taken as 5 DL. The separation distance between the standard duct and the second duct is controlled by the recommended throat width of 0.8 DL, as shown in Fig. 4b.

B. Converging–Diverging Channel in the Duct

The second duct and the standard duct form a converging–diverging channel starting from the trailing edge of the second (outer) duct located at about $X = 5\ DL$. The throat section's axial position is about 0.45 c, where c is the axial chord of the inner duct, as shown in Fig. 4b. The second duct width at the entrance of the converging–diverging duct is DL. The entrance to the converging–diverging channel is at the trailing-edge point of the second duct. There is a (vertically up) net flow in the converging–diverging duct of the DDF. This flow increases dynamic pressure at the converging–diverging duct entrance at $X = 5\ DL$ when the edgewise flight velocity increases. The diverging part of the channel flow between the standard and outer duct is essential in this novel approach because this locally decelerating flow is instrumental in adjusting the wall static pressure gradient around the lip section of the leading edge of the standard duct. The self-adjusting dynamic pressure of the inlet flow into the converging–diverging duct is directly proportional to the square of the edgewise flight velocity of the vehicle. The converging–diverging duct flow is also in a vertically up direction near the inner duct's leading edge. The intermediate channel flow is vertically down when one moves away from the frontal section of the vehicle. This
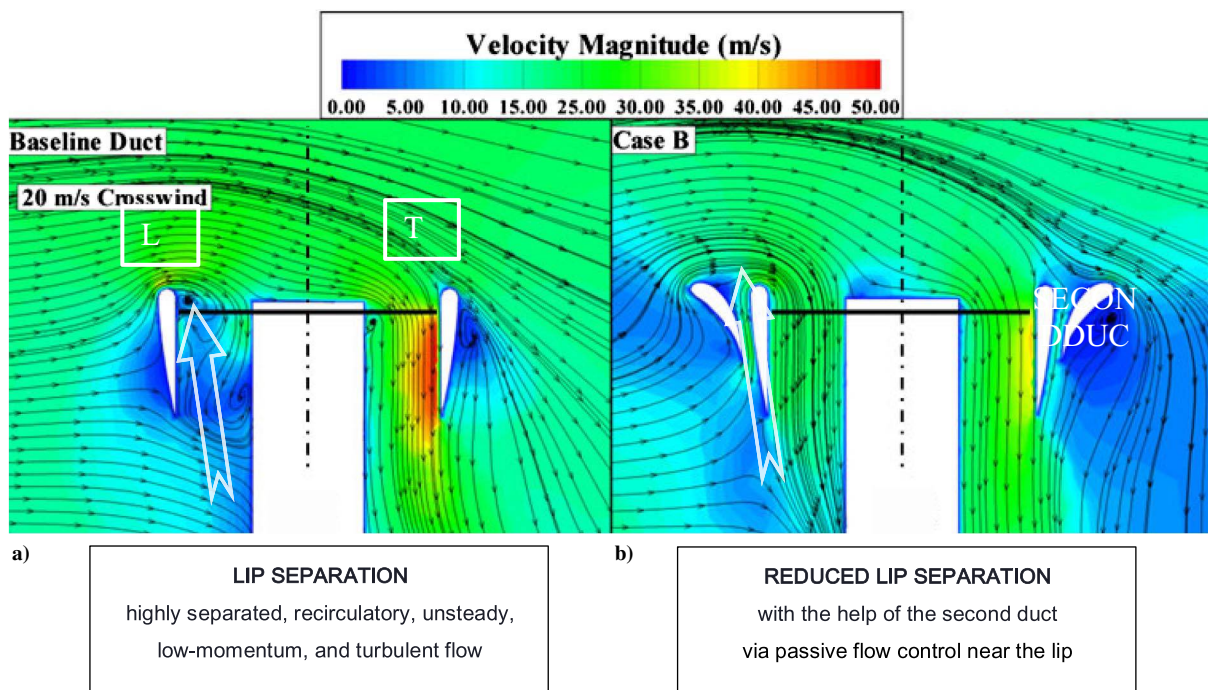

Fig. 3 Separated flow near the forward lip section of a "standard" ducted fan (left) and the flow improvements from the novel concept double-ducted fan (DDF) at 9000 rpm, colored by the magnitude of velocity.

Fig. 4   a) Baseline duct airfoil definition in a standard ducted fan arrangement, and b) double-ducted dan (DDF) case B geometry as a novel concept.

downflow induced by the local total pressure field near the second duct entrance is likely to generate measurable additional thrust force for the DDF-based vehicle. One should note that the second duct entrance near the leading edge has an inlet dynamic pressure scaling with edgewise flight speed. The exit of the second duct near the trailing side is a wake region.

C.   Various Possible Double-Ducted Fan Configurations

Figures 5 and 6 show the standard duct and three possible double-ducted fan (DDF) design variations as vertical cross sections. Case A is shown in Fig. 3b (termed as the tall DDF). The tall DDF can generate a measurably higher thrust in the hover position than the standard duct containing an identical rotor. However, due to the extended axial chord of the outer duct in edgewise flight, the nose-up pitching moment generation is amplified in this design. This design has a throat section located at the trailing edge of the duct airfoils. Because the axial chord of the outer duct is longer than that of the inner duct, this design may have a drag penalty when compared to the standard ducted fan.

Figure 6a shows the most effective double-ducted fan (DDF) configuration, case B. It can generate a significant amount of thrust compared to that of the standard ducted fan configuration. Another critical characteristic of case B is its ability to operate without amplifying the nose-up pitching moment of the vehicle in an edge-wise flight. The authors analyzed this configuration in great detail, mainly because of its combined ability to enhance thrust and reduce nose-up pitching moment in edgewise flight without a significant

drag penalty. Figure 6b shows an eccentric-double-ducted-fan con-cept. This design approach requires a movable outer duct to control the vehicle's intermediate duct's throat area for a better optimized edgewise flight performance. The variable throat mechanism intro-duced in this concept provides a greater range of operation in a DDF type vehicle offering a more accurate lip flow control over a much wider edgewise flight velocity range. Figure 6b shows an almost blocked second duct near the leading edge of the vehicle. The eccentric double-ducted fan of Fig. 6b is useful for very low edgewise flight velocities. It is required that the throat area is enlarged by moving the outer duct as the edgewise flight velocity is increased. Although an almost optimal lip separation control is possible with an eccentric DDF, its mechanical complexity and the weight penalty are apparent. The outer duct airfoil definition of this concept is the same as case B, described in detail in Fig. 6a. Applying the second duct's flow control feature only near the leading side of the vehicle is also a possibility.

IV.   Research Methodologies

A three-dimensional simulation of the mean flowfield around the ducted fan was performed using a custom-developed actuator disk model based on the radial equilibrium theory implemented into the commercial code ANSYS-FLUENT. The specific computational system solves the Reynolds-averaged Navier–Stokes (RANS) equa-tions using a finite volume method. A set of "user-defined functions" was developed and linked with the general-purpose RANS solver.

Fig. 5   An overview of configurations studied: a) baseline ducted fan (standard duct), and b) case A tall double-ducted fan (DDF).
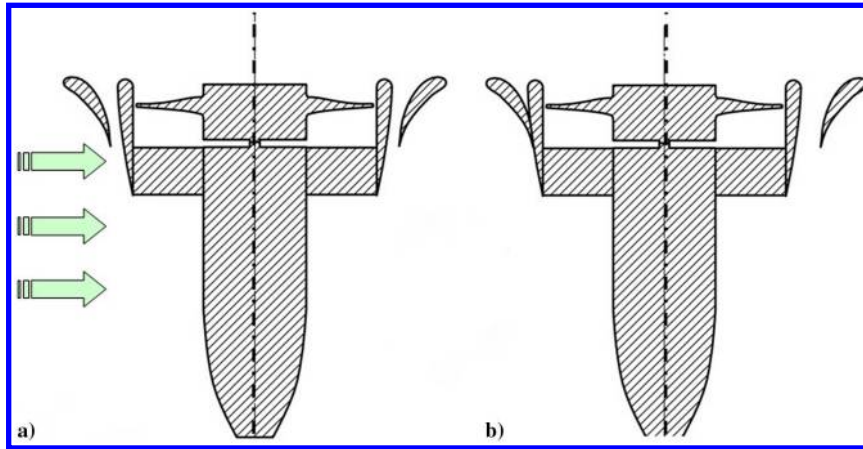
Fig. 6 An overview of configurations studied: a) case B short double-ducted fan, and b) eccentric double-ducted fan.

A. Reference/Baseline Ducted Fan Experiments

A DC electric motor of the brushless type drives the five-bladed ducted fan rotor for the reference/baseline fan. This motor is speed controlled by an electronic speed control system. The high-efficiency electric motor driving the fan can deliver 1.5 kW power (2.14 HP) and spin at 9000 rpm supplied to the motor. Figure 7 shows the five-bladed reference fan that is used in the present DDF conceptual development effort. The relatively poor edgewise flight characteristics of the reference ducted fan, as shown in Fig. 7, are significantly improved via the new double- ducted fan (DDF) concept. Table 1 presents the pertinent geometrical specifications of the reference ducted fan rotor designed for uninhabited aircraft. This fan unit is manufactured from carbon composite material and has six outlet guide vanes at the fan's exit to remove some of the swirl existing at the rotor's exit. There exists a tail cone to cover the motor surface and hide the electrical wiring during wind-tunnel experiments. All computational 3-D flow simulations of the reference duct, including the rotor flowfield, are performed at 9000 rpm using the geometry shown in Fig. 7. Akturk and Camci explained their validation effort of the RANS-based CFD model developed for this study in [30,31]. They focused on the grid generation features, the grid sensitivity results, the turbulence model, and experimental validation cases for the current DDF computations.

B. Computational Model, a RANS-Based Ducted Fan Flow Solution Including a Rotor Simulation

A simulation of the mean flowfield around and inside the ducted fan was performed using a computational fluid dynamics software
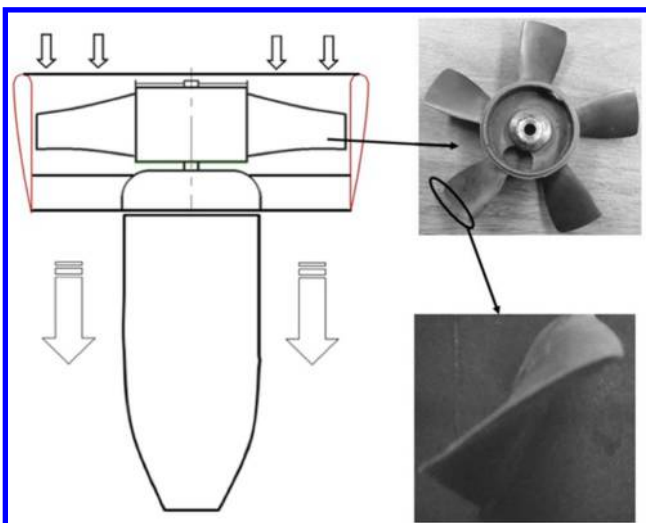
Table 1 Geometric specifications of the baseline ducted fan

Rotor hub diameter	52 mm		
Rotor tip diameter	120 mm		
Blade height h	34 mm		
Tip clearance t/h	5.8%		
Max blade thickness at rotor tip	1.5 mm		
Tail-cone diameter	52 mm		
Tail-cone length	105 mm		
Rotor blade section properties			
	Hub	Midspan	Tip
Blade inlet angle β_1	60 deg	40 deg	30 deg
Blade exit angle β_2	30 deg	45 deg	60 deg
Blade chord	32 mm	30 mm	28 mm

ANSYS-FLUENT [35]. The current computations used an in-house-developed "user-defined function" (UDF) for the rotor flow-field simulation. The specific computational system solved the 3-D Reynolds-averaged Navier–Stokes equations using a finite volume method. The numerical solution of the transport equations employed an unstructured computational mesh. The most complex and time-consuming computational effort could be modeling unsteady/viscous/turbulent flow in and around the fan rotor, employing a high-fidelity 3-D model using a sliding mesh technique. A sliding mesh type of solution is usually lengthy and requires significant computing resources in the edgewise flight mode when an axisymmetric flow assumption is not applicable. The current RANS computations used a custom-developed, in-house rotor flow model to generate the fan rotor's general inviscid flow features. All other flow regions other than the rotor section used a viscous flow computation incorporating a k-ε turbulence model. A more detailed description of the computational model from the authors of this paper, including grid generation details, grid sensitivity, turbulence model, and experimental validation cases, can be found in [30,31].

C. Boundary Conditions for Hover Conditions

Figure 8 shows the specific boundary conditions and computational domain implemented in the solver for hover conditions. The duct and the tail-cone surfaces are considered solid walls with no-slip conditions. On the side surfaces, a symmetry condition is assumed. For the hover condition, a pressure inlet boundary is prescribed on the top surface. Atmospheric static pressure is specified on the top surface. Pressure inlet boundary is treated as a loss-free transition from stagnation to inlet conditions. The solver calculates the static pressure and velocity at the rotor inlet. Mass flux through the boundary varies depending on the interior solution and specified flow direction. The bottom surface boundary condition is of the type "pressure-outlet" for the hovering condition. The atmospheric static pressure of the environment is the pressure-outlet boundary value. An additional custom-developed "fan"-type condition was used for the implementation of the specific actuator disk model described in the next section.
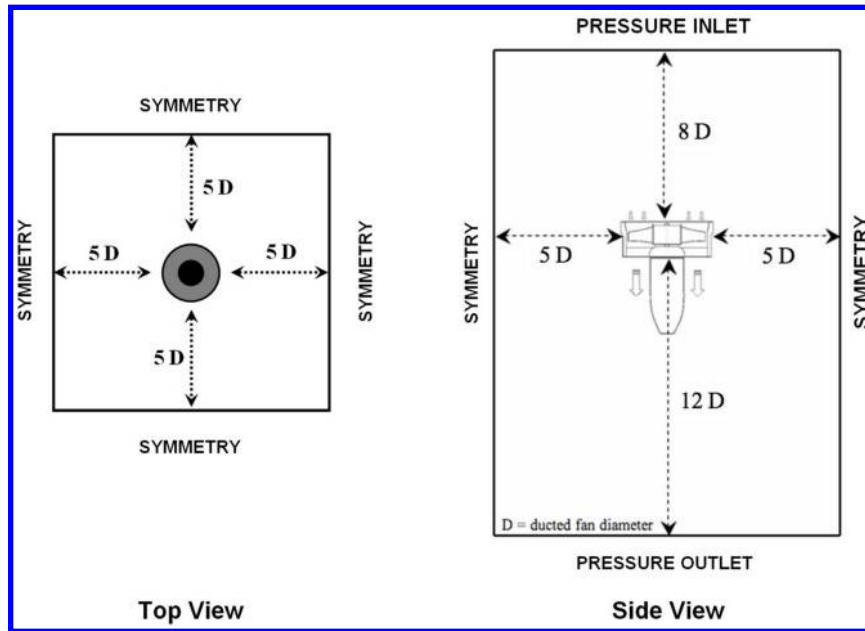

Fig. 7 Reference ducted fan assembly and fan rotor used for DDF development effort.

Fig. 8 Boundary conditions for hover.

D. Boundary Conditions for Edgewise Flight Conditions

Figure 9 shows the specific boundary conditions implemented in the solver for edgewise flight. Like hover conditions, the duct and tail-cone surfaces are considered solid walls with no-slip conditions. The windward side of the computational domain uses a velocity inlet boundary condition. Velocity and turbulent intensity at the windward side are prescribed. For the leeward side of the domain, an outflow condition is assigned. For the top, bottom, and remaining side surfaces, the symmetry boundary condition is designated. Like the hover condition, the *fan*-type condition was set using a simplified "actuator disk model," replacing the ducted fan rotor. Details of the inviscid actuator disk model follow.

E. Rotor Flow Representation via a Custom Actuator Disk Model

A custom actuator disk model replaces the complex 3-D rotor flowfield in the rotating frame of reference. This inviscid custom-developed actuator disk model originates from the simultaneous use of the radial equilibrium equation, energy equation, and the conservation of angular momentum principle across the fan rotor. The radial

equilibrium equation is the force balance in the radial direction at a given axial position, balancing the pressure forces with the centrifugal force. The current simplified and easy-to-implement actuator disk model ignores the viscous effects. In this approach, a pressure change term is computed at each radial position of the rotor from hub to tip. The magnitude of the static pressure jump across the rotor is closely related to the stagnation enthalpy change from the rotor inlet to exit. The stagnation enthalpy increase from the rotor inlet to exit is the same as the rate of energy provided to the fluid by the rotor per unit mass flow rate of the duct flow. The conservation of the angular momentum principle and energy equation suggests that the magnitude of this jump is mainly controlled by the tangential (swirl) component $c_{\theta 2}$ of the flow velocity in the absolute frame of reference at the exit of the rotor and rotor angular velocity.

Figure 10 presents the ducted fan rotor's velocity triangles at the inlet (1) and exit (2). β_1 and β_2 are the blade inlet and exit angles measured from the axial direction. Because the tip Mach number (0.28) of the rotor is not in the compressible flow range, it is reasonable to assume that the internal energy at the rotor inlet e_1
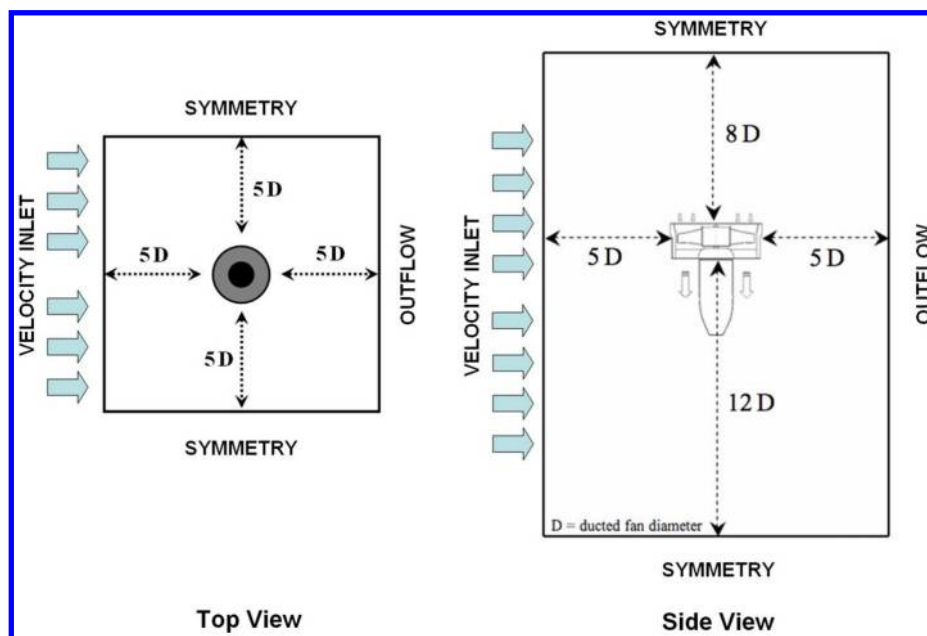

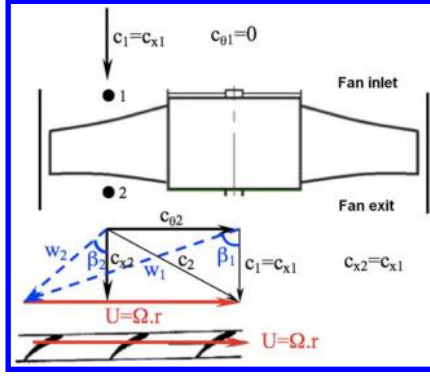**Fig. 9 Boundary conditions for edgewise flight.**

Fig. 10 Velocity triangles at the inlet and exit of the ducted fan rotor.

and exit e_2 is the same, $e_1 = e_2$. In a ducted fan rotor, it is realistic to assume that the "axial component" is also conserved from the inlet to exit $c_{x2} = c_{x1}$. The flow is considered axial at the rotor inlet where $c_1 = c_{x1}$ and $c_{\theta 1} = 0$ under design conditions. The relative velocity vector at the exit of the rotor w_2 is smaller than the relative velocity w_1 at the rotor inlet. Whereas the relative flow w_2 is diffusing in the relative frame of reference, the absolute flow velocity vector c_2 is accelerated at the rotor exit because of added energy to the flow by the rotor.

Equation (1) represents the change of stagnation enthalpy in the ducted fan rotor system. The right-hand side of this equation is the rate of work per unit mass flow rate of air passing from the rotor. The right-hand side is also the same as the product of the fan rotor's rotor torque and angular speed.

$$h_{o2} - h_{o1} = U(c_{\theta 2} - c_{\theta 1}) \text{ where } U = \Omega r \text{ and } c_{\theta 1} = 0 \quad (1)$$

$$(h_2 + c_2^2/2) - (h_1 + c_1^2/2) = U c_{\theta 2} \quad (2)$$

$$\left(e_2 + \frac{p_2}{\rho_2} + c_2^2/2 \right) - \left(e_1 + \frac{p_1}{\rho_1} + c_1^2/2 \right) \quad (3)$$

Equation (1) is a simplified form of the energy equation from the rotor inlet to the exit of the ducted fan unit. When $e_1 = e_2$ is substituted into Eq. (3) because of the incompressibility condition, the "Euler equation" or "pump equation" results in Eq. (4). A statement for calculating the static pressure jump between the rotor inlet and exit can be obtained using Eq. (4).

The determination of $c_{\theta 2}$ is performed by using the velocity triangles in Fig. 10. Because the blade inlet/exit angle distribution for 1 and 2 in the radial direction is known from the existing rotor geometrical properties, shown in Table 1, w_2 can be calculated from the assumption $c_{x2} = c_{x1} = c_1$. The absolute rotor exit velocity c_2 is determined by adding $U = \Omega r$ to w_2 in a vectorial sense.

$$\frac{1}{\rho}(P_{o2} - P_{o1}) = U c_{\theta 2} \quad (4)$$

$$(p_2 + \rho c_2^2/2) - (p_1 + \rho c_1^2/2) = U c_{\theta 2} \quad (5)$$

$$\Delta p = (p_2 - p_1) = \rho \left[U c_{\theta 2} - \frac{1}{2}(c_2^2/2 - c_1^2/2) \right] \quad (6)$$

Equation (6) allows enforcing a prescribed pressure jump across the rotor plane in the function of density, radial position, rotor angular speed Ω, and rotor exit swirl velocity $c_{\theta 2}$, c_1, and c_2. The rate of energy per unit mass flow rate added to the flow by the rotor is specified by the product $U c_\theta$, as shown in Eqs. (4) and (5). Equation (6) could be evaluated at each radial position between the rotor hub and tip, resulting in the radial distribution of the static pressure jump required by the general-purpose viscous flow solver. A user-defined function (UDF) in the general-purpose flow solver adequately prepares Δp using Eqs. (1–6). Further details of this approach, including the actuator disk, grid generation features, the grid sensitivity results, the turbulence model, and experimental validation, are explained in detail by Akturk and Camci [30,31].

V. Simulation Results and Discussion on DDF Flowfield in Edgewise Flight

A. Rotor Mass Flow Rate Improvements via the DDF Concept

Table 2 presents the computed rotor mass flow rate for all ducted fan types studied in this paper. In addition to hover conditions, the results are also offered for 10and 20 m/s edgewise flight velocities at 9000 rpm rotor speed, kept constant for all computations.

Flow simulations at constant rpm provide a basis for comparing the 3-D mean flow, fan thrust, nose-up pitching moment, total pressure, and static pressure fields. Although the rotor speed is constant for all computations, the amount of mechanical energy transferred to the air during its passage through the rotor varies. This variation is mainly because of the highly varying inlet flowfield into the ducted fan unit during hover, edgewise flight at 10 m/s, and 20 m/s. Table 2 also provides the computational estimates of thrust, nose-up pitching moment for hover, and edgewise flight conditions.

Figure 11 shows that the baseline duct suffers from a high level of inlet flow distortion at 10 and 20 m/s edgewise flight velocity. The overall mass flow rate passing from the ducted fan is reduced to 66% of the hover mass flow rate, as shown by the red line for 20 m/s edgewise flight. This significant limitation on the rotor mass flow rate is mainly due to the large separated flow region occurring downstream of the lip section of the leading side of the duct, as shown in Fig. 1. Although the leading side of the baseline duct passes a severely limited amount of air mass, the duct's trailing side can breathe at a better rate than the leading side. The leading side of the baseline duct is partially blocked at high edgewise flight velocities.

B. Baseline Duct Mass Flow Rate, Thrust, and Nose-up Pitching Moment

Table 2 contains nose-up pitching moment information for all flight regimes showing a measurable increase in pitching moment when the baseline vehicle moves at 10and 20 m/s in comparison to hover conditions. The nose-up pitching moment is measured with

Table 2 Rotor mass flow rate for all ducted fan configurations during hover and edgewise flight

|	Fan mass flow rate, kg/s	Thrust, N	Pitching moment, N.m	Flight condition
Baseline duct	0.30	3.04	0.00	No crosswind (hover)
Baseline duct	0.29	3.47	0.17	10 m/s crosswind
Baseline duct	0.20	3.11	0.27	20 m/s crosswind
		Modified ducts (DDF)		
Case A	——	——	0.00	No crosswind (hover)
Case A	0.31	4.93	0.37	10 m/s crosswind
Case A	0.26	5.07	0.83	20 m/s crosswind
Case B	——	——	0.00	No crosswind (hover)
Case B	0.30	3.72	0.16	10 m/s crosswind
Case B	0.28	4.86	0.29	20 m/s crosswind
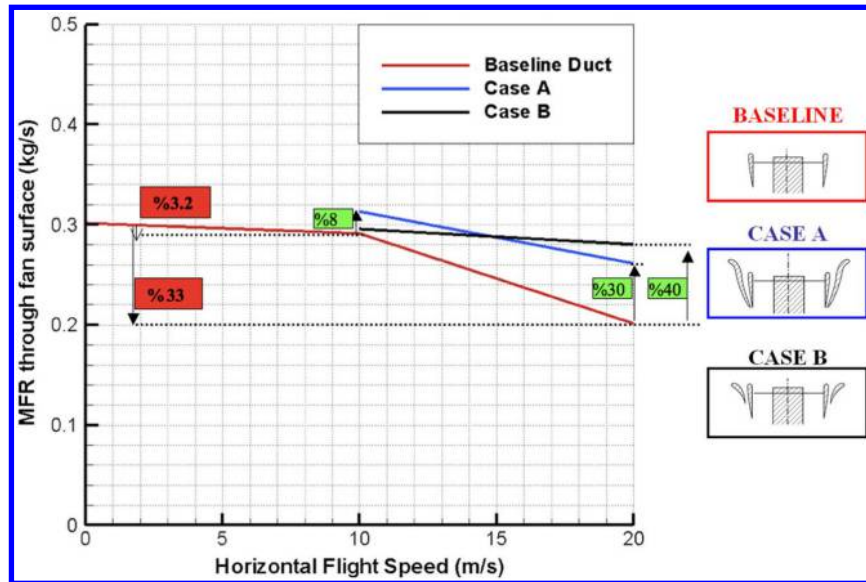
Fig. 11 Rotor disk mass flow rate vs edgewise flight speed at 9000 rpm.

respect to the center of gravity of the ducted fan unit for all cases. At 20 m/s edgewise flight condition, the predicted pitching moment (0.27 N.m) is 1.6 times that of the pitching moment (0.17 N.m) at 10 m/s flight velocity. The pitching moment generation on a typical ducted fan in edgewise flight is directly related to the extent of inlet lip separation, the impingement of the rotor inlet flow on the inner duct surface (aft shroud surface) on the trailing side of the duct. Imbalance of the rotor exit field between the leading side (low momentum) and trailing side (high momentum), and aerodynamic profiling of the outer duct surface, especially near the leading-side predicted baseline ducted fan thrust values at 10 and 20 m/s increase to 1.42 and 1.63 times the baseline duct's thrust under hover conditions, respectively. This relative thrust improvement is due to the baseline duct's specific external shape and modified rotor inlet conditions at elevated edgewise flight speed levels.

C. Mass Flow Rate Through Case A

The baseline duct's air-breathing character can be significantly improved by implementing the tall double-ducted fan (DDF) designated as case A, as shown in Fig. 11. Case A's mass flow rate is about 8% more than that of the baseline duct operating at the edgewise flight speed of 10 m/s. The rotor mass flow rate improvement for case A at 20 m/s is much more significant than that of the baseline duct operating at 20 m/s. A 30% improvement over the baseline duct is possible. This relative mass flow rate gain directly reduces inlet lip separation near the duct's leading side during edgewise flight.

D. Thrust from Case A

The predicted thrust for the tall double-ducted fan (DDF) case A is markedly higher than that of the baseline duct. At 10 m/s horizontal flight velocity, case A's thrust is about 1.42 times that of the baseline duct. Case A produces an augmented thrust value of 1.63 times that of the baseline duct when the flight velocity is elevated to 20 m/s. The reduction of the inlet lip separation results in an immediate improvement of the ducted fan exit flow near the leading side of the duct. The thrust improvements are due to both ducted fan exit flow improvements near the unit's leading side and the external aerodynamic shape of the outer duct. The leading side of the DDF case A rotor plane breathes air from the inlet at a much improved rate than that of the baseline duct. The tall (DDF) case A also entrains a measurable amount of air into the outer duct from the unit's inlet area, especially near the trailing side. The flow in the outer duct is in the opposite direction to the rotor flow near the leading side. However, the outer duct flow for the circumferential positions away from the duct's leading side is in the same direction as the main rotor flow direction.

Additional thrust augmentation is possible in the outer duct at positions away from the leading edge.

E. Nose-Up Pitching Moment Characteristics of Case A

The tall (DDF) case A is an excellent thrust producer at high edgewise flight velocities. However, it tends to amplify the unwanted nose-up pitching moment mainly because of the outer lip's external shape at elevated edgewise flight velocities. The pitching moment predicted at 10 m/s is about 2.2 times that of the baseline duct. At 20 m/s, the pitching moment produced by case A is about 3.1 times that of the baseline duct value. The reason the short-ducted-fan case B was designed was the need to reduce the unwanted pitching-up-moment generation unique to case A.

F. Case B as an Effective DDF Design with Highly Reduced Nose-Up Pitching Moment

Case B, as previously shown in Figs. 6b and 14, is a shorter version of the double-ducted fan design concept. Case B is designed to produce a significantly reduced nose-up pitching moment when compared to case A. Another goal with case B is to obtain similar thrust gains over the baseline duct. The short double-ducted fan (DDF) case B controls the lip separation as effectively as the tall (DDF) case A without producing a high nose-up pitching moment. The airfoil geometry forming the outer duct has an axial chord length of about half of the inner duct's axial chord (also termed standard fan or baseline fan). A detailed description of obtaining a short double-ducted fan (DDF) case B is given in Fig. 4b, starting from a baseline duct. Figure 11 indicates that case B's mass flow rate improvement (black line) is very similar to case A (blue line). The short (DDF) case B's sensitivity to increasing edgewise flight velocity is much less than the tall (DDF) case A. As shown in Fig. 4b, the second duct's (case B) implementation enhances the lip separation-controlled flight zone further into higher edgewise flight velocities. The thrust values predicted for the short (DDF) are much higher than the baseline duct predictions at 10 and 20 m/s. There is a slight reduction in thrust when compared to the tall (DDF) case A. The most significant property of case B is its ability to control nose-up pitching moment effectively. The pitching moment generation for the short (DDF) case B is very much suppressed compared to tall (DDF) case A. Case B nose-up pitching moments are about the same as the values predicted for the baseline duct.

The short (DDF) concept described in Fig. 6a is a highly effective scheme for improving the lip separation-related inlet flow distortion problem for the rotor of a ducted-fan-based VTOL vehicle. Case B can improve thrust without increasing the nose-up pitching moment generation. Because the leading side of the fan

exit jet is well balanced against the exit jet's trailing side, control surfaces at the exit of the ducted fan function much more effectively for the short (DDF) case B.

VI. A Comparison of Local Velocity, Streamlines, and Total Pressure for All Three Ducts

As part of the (DDF) concept validation, local flowfield details, including the magnitude of velocity, streamlines, and total pressure distributions, are presented over a surface passing through the duct leading edge, the rotation axis trailing edge of the duct system. Comparisons of the specific (DDF) design against the corresponding baseline duct at 9000 rpm are discussed using the preceding computational procedures. In this section, the baseline duct, case A (the tall DDF), and case B (the short DDF) results are compared and discussed.

A. Case A Tall (DDF) vs Baseline Duct Results at 10 and 20 m/s

Figure 12 compares the tall double-ducted-fan flowfields as case A and the baseline duct. A slight forward lip separation is observed at 10 m/s edgewise flight velocity. The tall double-ducted-fan case A produces an enhanced thrust level of 1.73 times that of the baseline

ducted fan at 10 m/s. The mass flow rate of case A at 9000 rpm is also enhanced compared to the baseline ducted fan, as shown in Fig. 13. The total pressure distributions clearly show the low-momentum regions due to inlet lip separation and hub corner separation on the rotor disk inlet surface, as shown by dark blue areas.

The tall ducted fan reduces the low-momentum flow areas downstream of the inlet lip and hub corner compared to the baseline duct. Although the "hub corner separation" area is relatively smaller than the inlet lip separation area, the flow blockage created by the hub corner separation affects the rotor's flow downstream, as shown in Fig. 13. The total pressure imbalance observed downstream of the rotor for the baseline duct is significant. The tall double-ducted-fan case A slightly improves the total pressure on the rotor exit flow's leading side for 10 m/s edgewise flight velocity.

Figure 13 explains the effect of inlet flow distortion in the baseline duct and tall double-ducted- fan design at 10 m/s edgewise flight velocity using rotor exit total pressure predictions. The light green zone near the leading side of the baseline ducted fan shows the highest aerodynamic loss level resulting from inlet lip separation at 10 m/s. This area is where the inlet flow tends to separate because of the duct lip's existence near the leading side. The fan inlet surface also has another aerodynamic loss region (green) downstream of the "hub
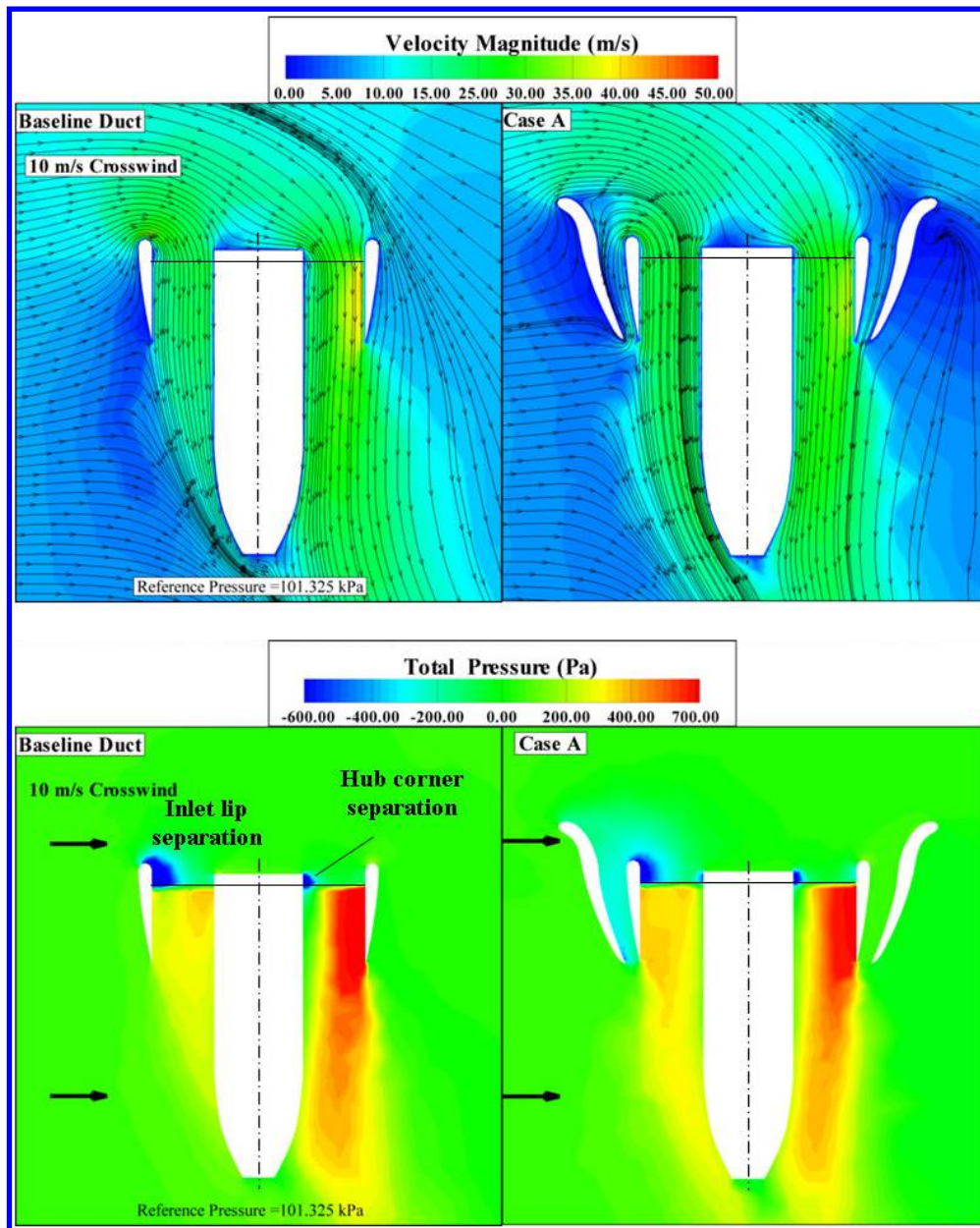

Fig. 12   Velocity magnitude and total pressure distribution, baseline duct vs case A double-ducted fan (DDF) at 10 m/s edgewise flight velocity.
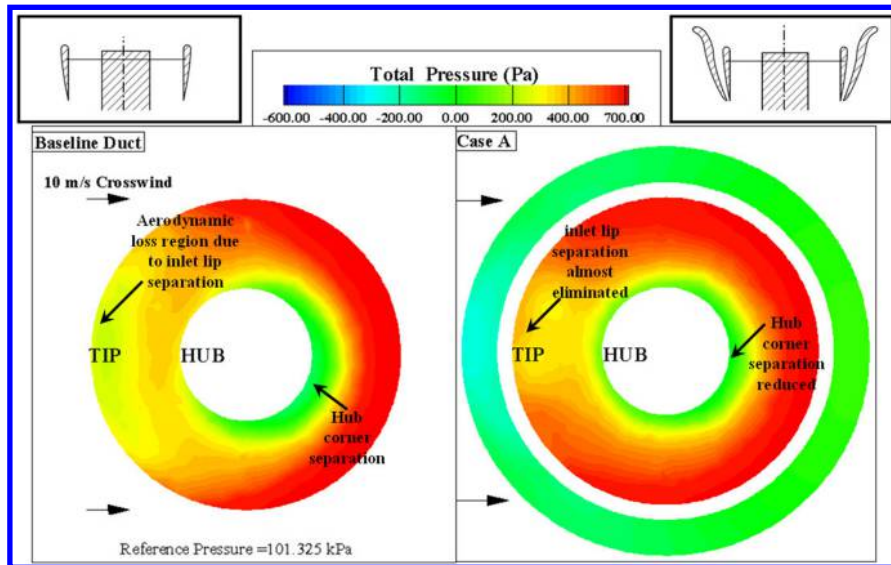
Fig. 13   Total pressure distribution at rotor exit plane, baseline duct vs case A tall double-ducted fan (DDF) at 10 m/s edgewise flight velocity.

corner" on the duct's trailing side. Figure 13 shows the beneficial influence of the tall double-ducted-fan design case A. The aerodynamic loss areas in the baseline duct distribution are effectively reduced in the tall double-ducted-fan design. The red total pressure zone near the baseline duct's trailing side shows the highest level of total pressure over the rotor exit plane. The trailing side tends to pass most of the inlet mass flow rate, including the fluid skipping over the lip separation region. Most standard ducted fans in horizontal flight or at a high angle of attack have this common flow feature. The aft part of the fan usually generates additional drag force because of this red high total pressure zone at the exit plane. The tall double-ducted-fan's implementation makes the total pressure distortion much more balanced between the leading and trailing sides. The inlet flow distortion is effectively dealt with by implementing the second duct configuration called case A; see Fig. 13.

Figure 14 shows the separated flow zone's highly adverse character behind the inlet lip section in the baseline duct when edgewise flight velocity increases to 20 m/s. The flow tends to separate behind the hub corner on the trailing side of the duct. Figure 14 demonstrates the severe flow blockage by the existence of a large separated flow zone, and the flow is unnecessarily induced into the trailing side of the duct. The imbalance in the local mass flow rate between the leading side of the duct and the duct's trailing side at 20 m/s is much more apparent than the 10 m/s results. Figure 14 displays the significant flow improvement near the lip separation area for the tall double-ducted-fan (DDF) case A. The recirculatory flow is virtually eliminated downstream of the lip. The duct's leading side starts breathing effectively because of case A's ability to eradicate inlet flow distortion near the leading side. The (DDF) case A results show a low-momentum region as a three-dimensional wake behind the vehicle at 20 m/s edgewise flight velocity. The outer duct flow near the leading side is in a direction opposite to the rotor flow direction. The outer duct flow near the leading side is an essential driver of the (DDF) concept because of its highly significant role in alleviating the inner lip region separated flow conditions. The outer duct flow smoothly reverses into the rotor flow direction away from the leading side.

The rotor exit plane total pressure distribution shown in Fig. 15 (DDF) case A reveals a significant lip separation improvement leading to a much more uniform inlet flow distribution between the leading and trailing sides of the inner duct. The DDF local flow distribution at the rotor exit is much improved when compared to the baseline duct. Hub corner separation area is also reduced in (DDF) case A. Except for the leading side, the second duct contributes to the thrust generation because of the measurable outer duct flow observed in this area.

B.   Case B Short (DDF) vs Baseline Duct Results at 10 and 20 m/s

Figures 16 and 17 show the most effective double-ducted-fan (DDF) treatment results obtained for an edgewise flight velocity of 10 m/s. A detailed geometrical definition of the short double-ducted-fan (DDF) case B was discussed in Fig. 4b.

The short DDF can improve thrust relative to the baseline case *without producing a significant nose-up pitching moment* by effectively reducing inlet lip separation and hub corner separation areas. The short double-ducted-fan configuration is a self-adjusting lip separation control system preserving its separation control features in a wide range of edgewise flight velocities. The total pressure distribution presented in Fig. 16 for 10 m/s flight velocity shows the short DDF design's effectiveness. The total pressure imbalance between the leading side and trailing side is almost eliminated, in addition to the area reduction of the separated flow areas (dark blue). The leading side of the inner duct of the short DDF case B breathes at a much-improved rate as compared to the baseline case. The red high total pressure areas provide a well-balanced fan exit jet near the fan's leading and trailing sides.

Figure 17 indicates a high level of rotor exit total pressure uniformity for case B compared to the strong flow distortion generated by the baseline duct. The lip separation and hub corner separation control are highly effective at 10 m/s flight velocity for the short double-ducted fan. The total pressure values between the leading and trailing sides are much better balanced in case B, as shown in Fig. 17.

When the short double-ducted-fan arrangement (DDF) case B is evaluated at 20 m/s flight velocity, the loss elimination features near the leading-side lip, hub corner area are much apparent. Highly separated lip region flow, adversely blocking the leading side of the inner duct, is successfully dealt with the flow control features of the short (DDF), as shown in Figure 18. A well-balanced short (DDF) exit flow provides a higher level of thrust than the baseline duct. The flow improvements and thrust enhancement from the short (DDF) come with almost no additional nose-up pitching moment generation than the baseline, as explained in Table 2 and Fig. 18. Figure 19 illustrates the highly effective inlet flow distortion control ability of the short ducted fan. A vehicle using the short (DDF) concept as shown as case B generates a higher level of thrust with a well-balanced ducted fan exit flow without excessive generation of nose-up pitching moment. This approach results in improvements in the control surfaces' performance and range because the ducted fan's energy efficiency is increased. The elimination of severe inlet flow distortion is likely to improve the rotor exit flow quality before further interaction with vehicle control surfaces.
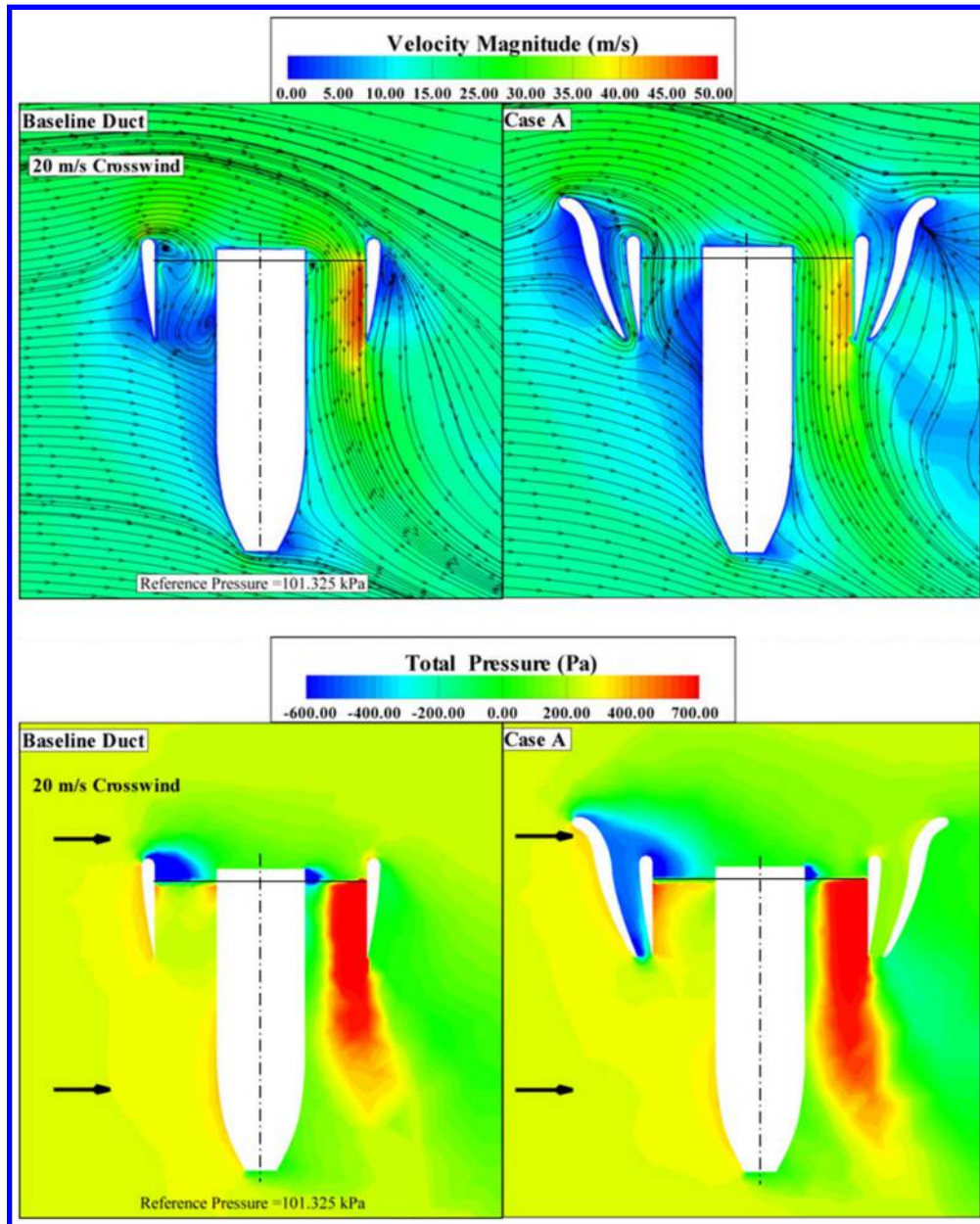
Fig. 14 Velocity magnitude and total pressure distribution, baseline duct vs case A tall double-ducted fan (DDF) at 20 m/s edgewise flight velocity.
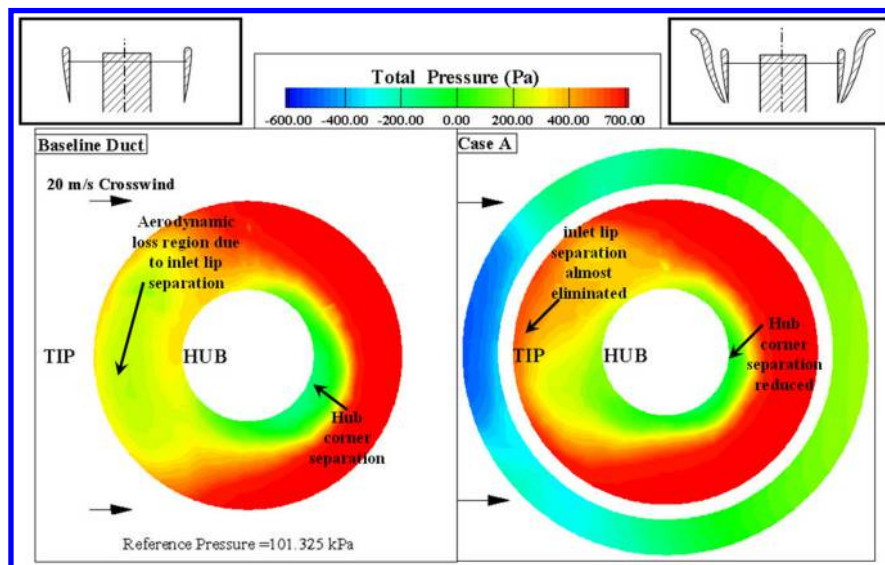

Fig. 15 Total pressure distribution at rotor exit plane (horizontal) baseline duct vs case A tall double-ducted fan (DDF) at 20 m/s edgewise flight velocity.
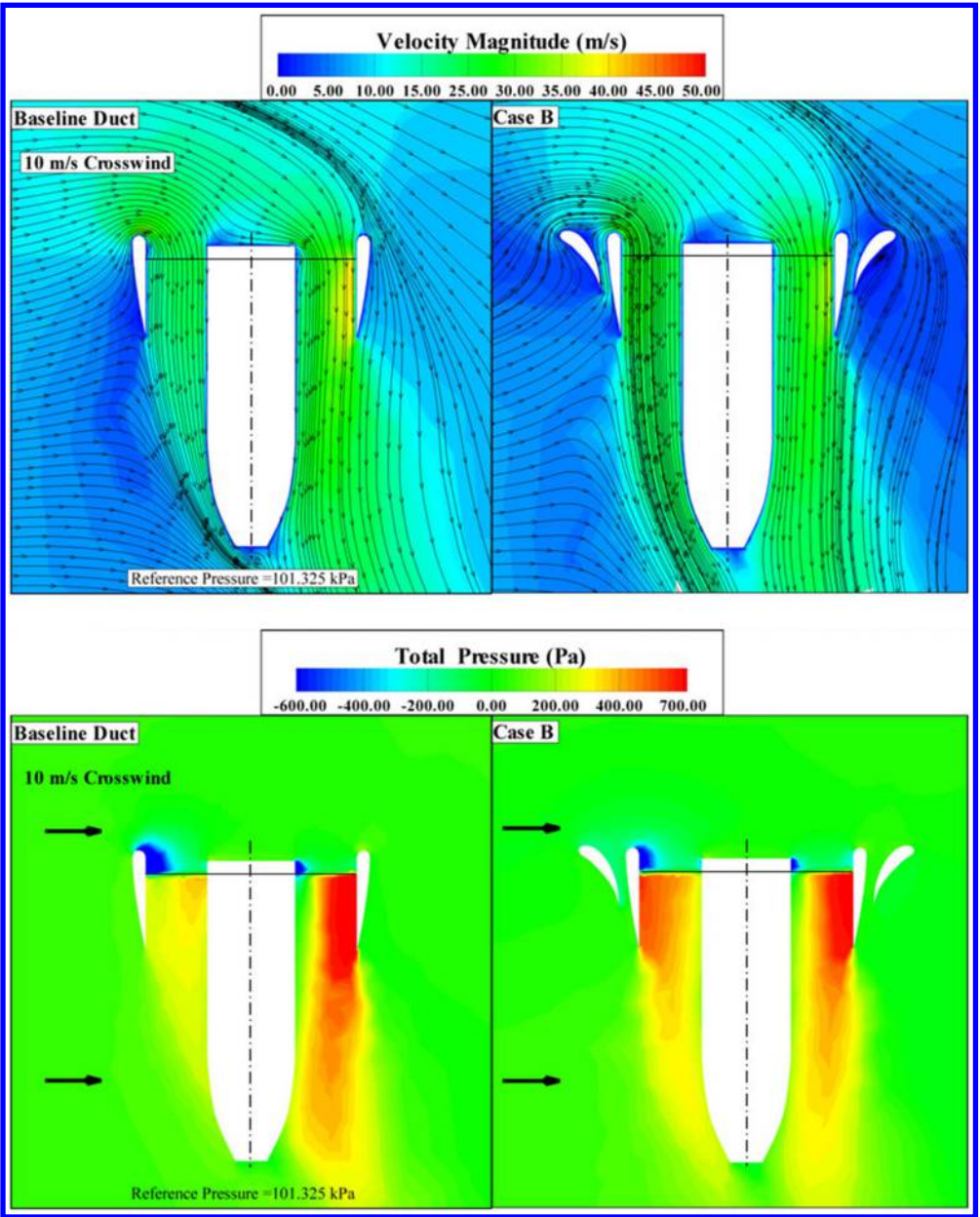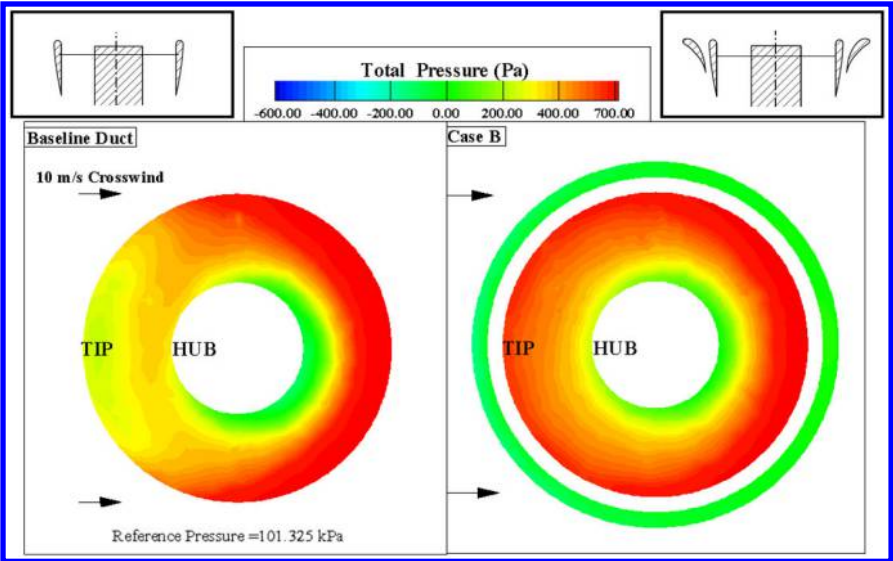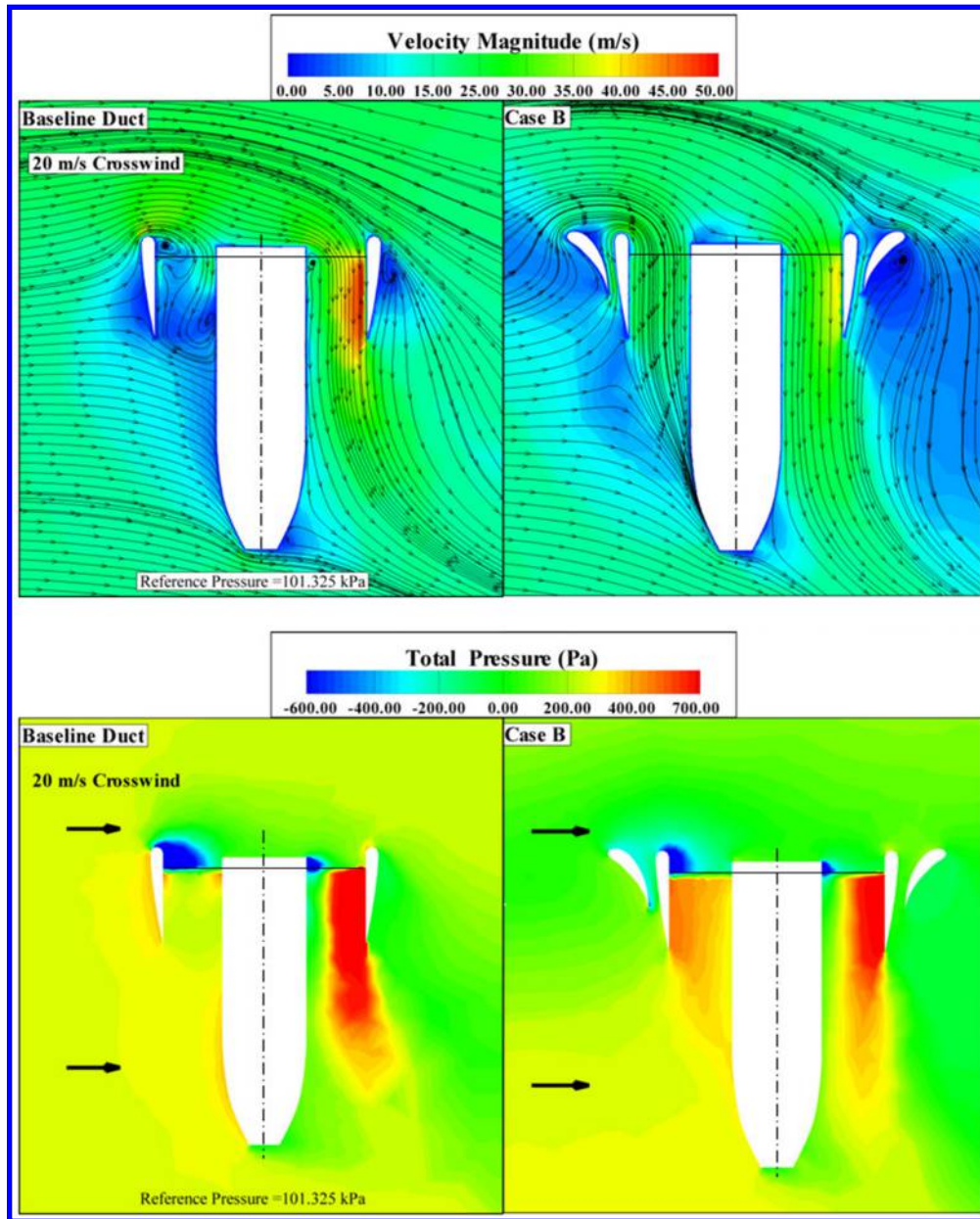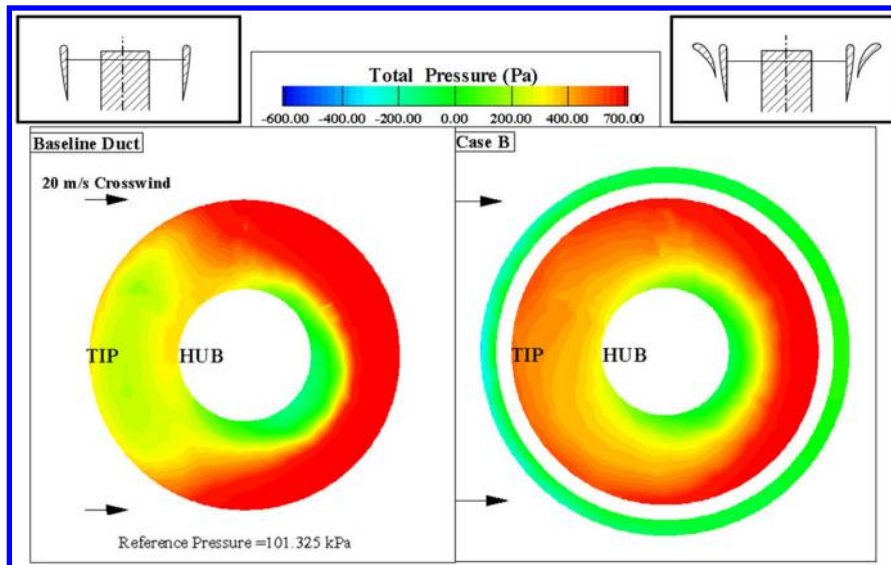
Fig. 16   Velocity magnitude and total pressure distribution, baseline duct vs case B short double-ducted fan (DDF) at 10 m∕s edgewise flight velocity.

Fig. 17   Total pressure distribution at rotor exit plane (horizontal) baseline duct vs case B short double-ducted fan (DDF) at 10 m∕s edgewise flight velocity.

Fig. 18   Velocity magnitude and total pressure distribution, baseline duct vs case B short double-ducted fan (DDF) at 20 m∕s edgewise flight velocity.

Fig. 19   Total pressure distribution at rotor exit plane (horizontal) baseline duct vs case B short double-ducted fan (DDF) at 20 m∕s edgewise flight velocity.

C.   Local Flow Improvements for Inner Lip Region Flow Separation Reduction (DDF)

This section aims to obtain local static pressure distribution of the inner duct in a DDF configuration. A comparison against the baseline duct effectively demonstrates the extent of local adverse pressure gradient zones near the duct lip section in Figs. 20 and 21. The lowercase characters represent the "rotor side" locations, and the uppercase characters show the "outer side" sampling locations for static pressure and skin friction coefficient on the inner duct airfoil section. The outer side denotes the channel between the baseline duct and the secondary duct.

D.   Static Pressure Distribution Around the Lip Section of the Baseline Duct

Figure 21 shows the static pressure distribution for the baseline duct and DDF case B for an edgewise flight velocity of 20 m/s. The distributions presented in Fig. 21 are plotted around the airfoil of the baseline duct. The pressure gradient occurring around the leading-edge radius of the inner duct is the most significant parameter controlling the leading-edge lip separation problem's severity level. Point $x = X/c = 0$ shows the leading edge, and $x = X/c = 1$ shows the baseline duct airfoil's trailing-edge location. The external flow stagnates on the baseline duct airfoil at point D, as shown in Fig. 21. The approaching flow to the duct is divided into a stream reaching up to the leading edge and a second stream approaching down to the trailing edge of the duct airfoil at point D. The static pressure from point D to J remains almost constant. The external flow slightly accelerates to the leading-edge point from point C to A for the baseline duct. There is a substantial acceleration zone between point A and the leading-edge point O, as clearly shown by the favorable pressure gradient between points A and O. This is the area within the leading-edge diameter of the inner lip section. The geometrical leading-edge point O is the minimum pressure point for the baseline duct airfoil. The flow on the lip's inner side sees a strong adverse pressure gradient around the leading- edge circle. The strong flow separation character shown in Fig. 21 is mainly due to the strong adverse pressure gradient affecting the boundary-layer growth between points O, a, and finally, b. The rotor process described in Eqs. (1–6) results in the sudden pressure rise on the baseline duct's inner part between b and c.

E.   Static Pressure Distribution Around the Lip Section of the Double-Ducted Fan (DDF)

Figure 21 also shows the static pressure distribution around the short double-ducted-fan (DDF) case B lip section. The vertical upward channel flow near the outer duct section's leading side is induced by the external flow's dynamic pressure in edgewise flight. The vertically upward flow exists in a narrow leading-edge region, as shown in the figure. The outer duct flow that is proceeding vertically up generates a unique wall static pressure distribution in a converging–diverging channel. The external flow in horizontal flight stagnates on the shorter outer airfoil and turns upward toward the leading edge of the outer duct airfoil. Most of the flow stagnating at the lower part of the vehicle is directed toward the converging–diverging channel of the outer duct. There is a broad stagnation region between points J and H on the outer side of the inner duct. The flow accelerates vertically toward the throat section of the outer duct near D. The flow after the throat section smoothly decelerates up to point A close to the leading-edge circle of the leading edge. The existence of the diverging channel is responsible for a much softer acceleration around the leading-edge diameter of the lip section between A and O. The flow is still accelerating when it is passing through the geometrical leading-edge point O. The minimum pressure point (M.P.) in (DDF) configuration is on the inner side of the lip section at $x = X/c = 0.03$ in contrary to the baseline duct location O. The flow starts decelerating after M.P. The adverse pressure gradient region after the minimum pressure point M.P. in (DDF) is much shorter, and the adverse pressure gradient between (M.P.) and point a is much milder than that of the baseline duct. Figure 21 clearly shows the favorable modified nature of the static pressure distribution around the lip section of (DDF), leading to eliminating the severe inlet lip separation region that is unique to the baseline duct in edgewise flight. The (DDF) approach is instrumental in controlling the inner lip flow separation originating from the adverse pressure gradient region.

VII.   Partial DDF and a Fan-in-Wing Implementation for Future VTOL Vehicles

A.   Partial DDF (PDDF)

The addition of the second duct around the fan's 360° circumference (case B) inherently increases the VTOL vehicle's weight. Although this second duct existing all around the fan can be manufactured from lightweight materials such as a composite skin, inflatable duct, or thin sheet metal, it is possible to benefit from the DDF concept by a local implementation only near the leading side. The current investigation reveals that the second duct manufactured as a partial circumferential segment, shown in Fig. 22, is also highly effective in controlling inlet lip separation in edgewise flight. The PDDF computationally evaluated in this study has a 100° partial coverage near the leading side, as shown in Fig. 22. Figures 23a and 23b present a quantitative comparison of the partial double-ducted fan (PDDF) against the DDF having a complete 360° second duct.
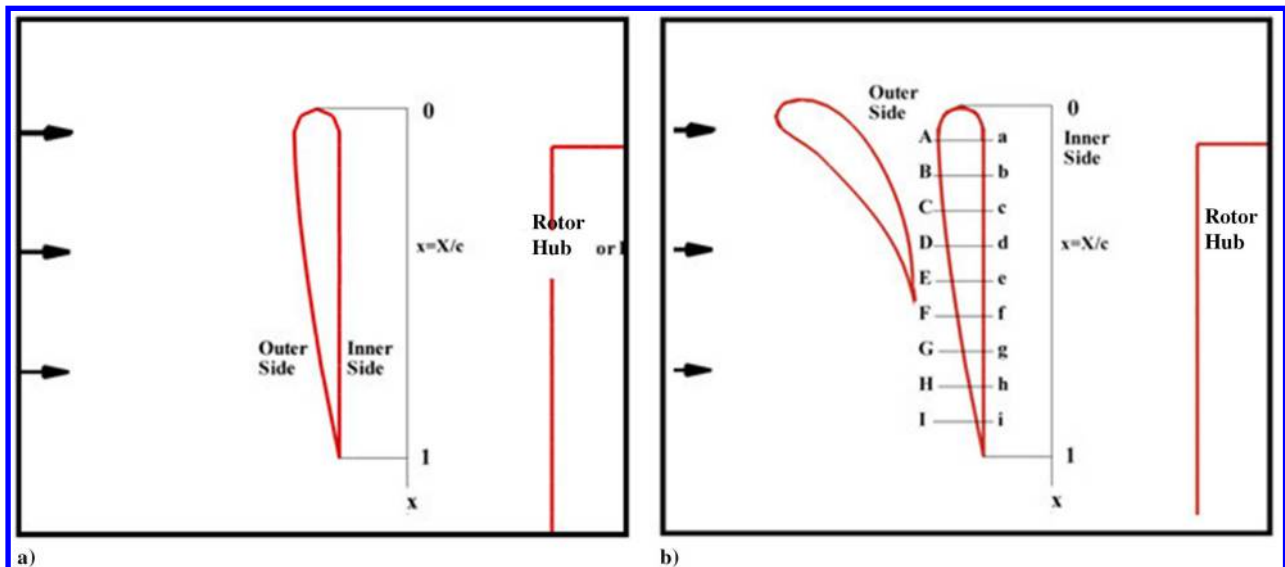

Fig. 20   Sampling locations for static pressure and skin friction coefficient computations near the leading side of the inner duct for (DDF) case B.
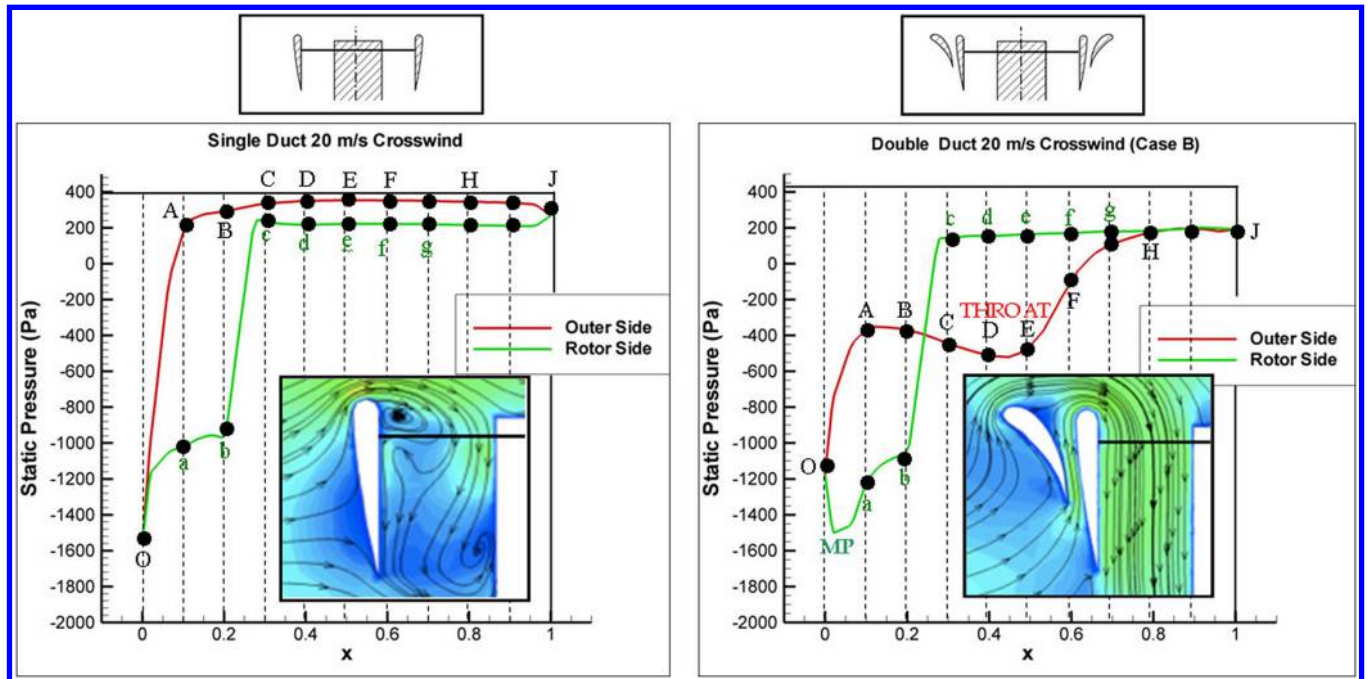
Fig. 21   Comparison of the static pressure distribution on the baseline lip section and inner duct lip section of the (DDF) case B airfoil.
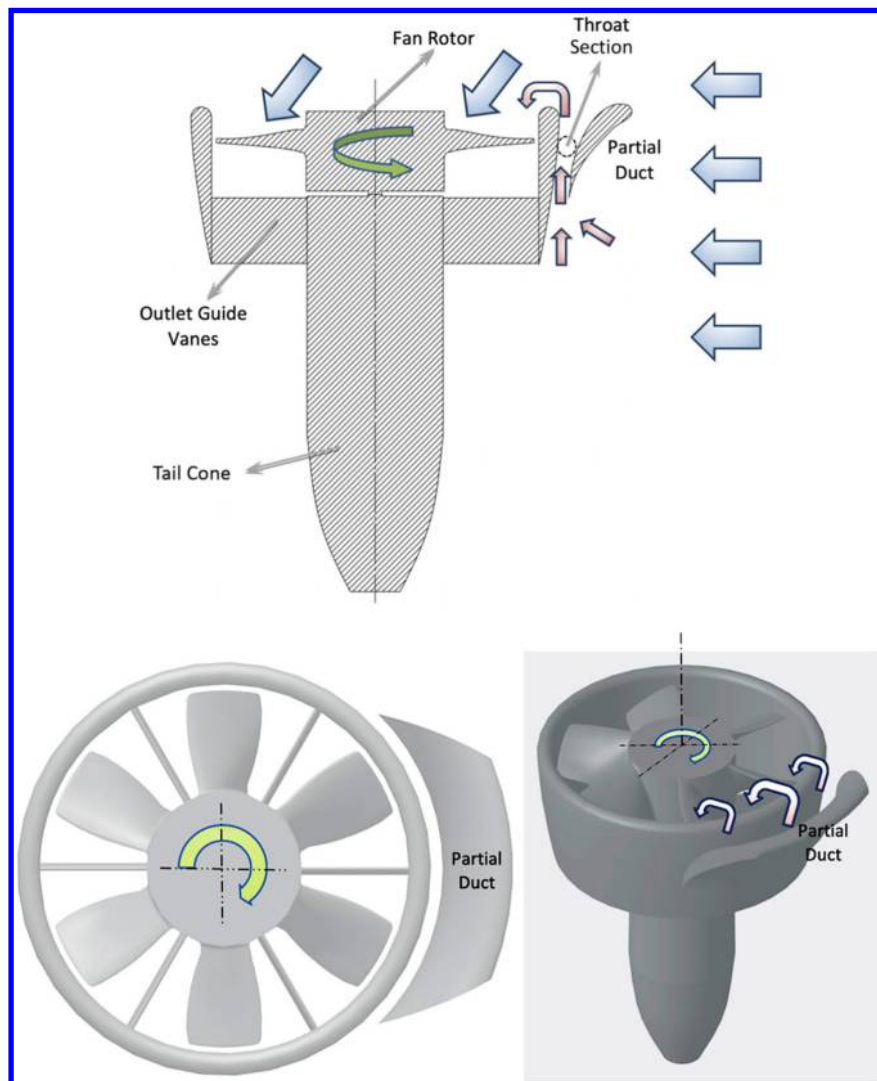

Fig. 22   Partial double-ducted fan (PDDF) without a 360° second duct usage.
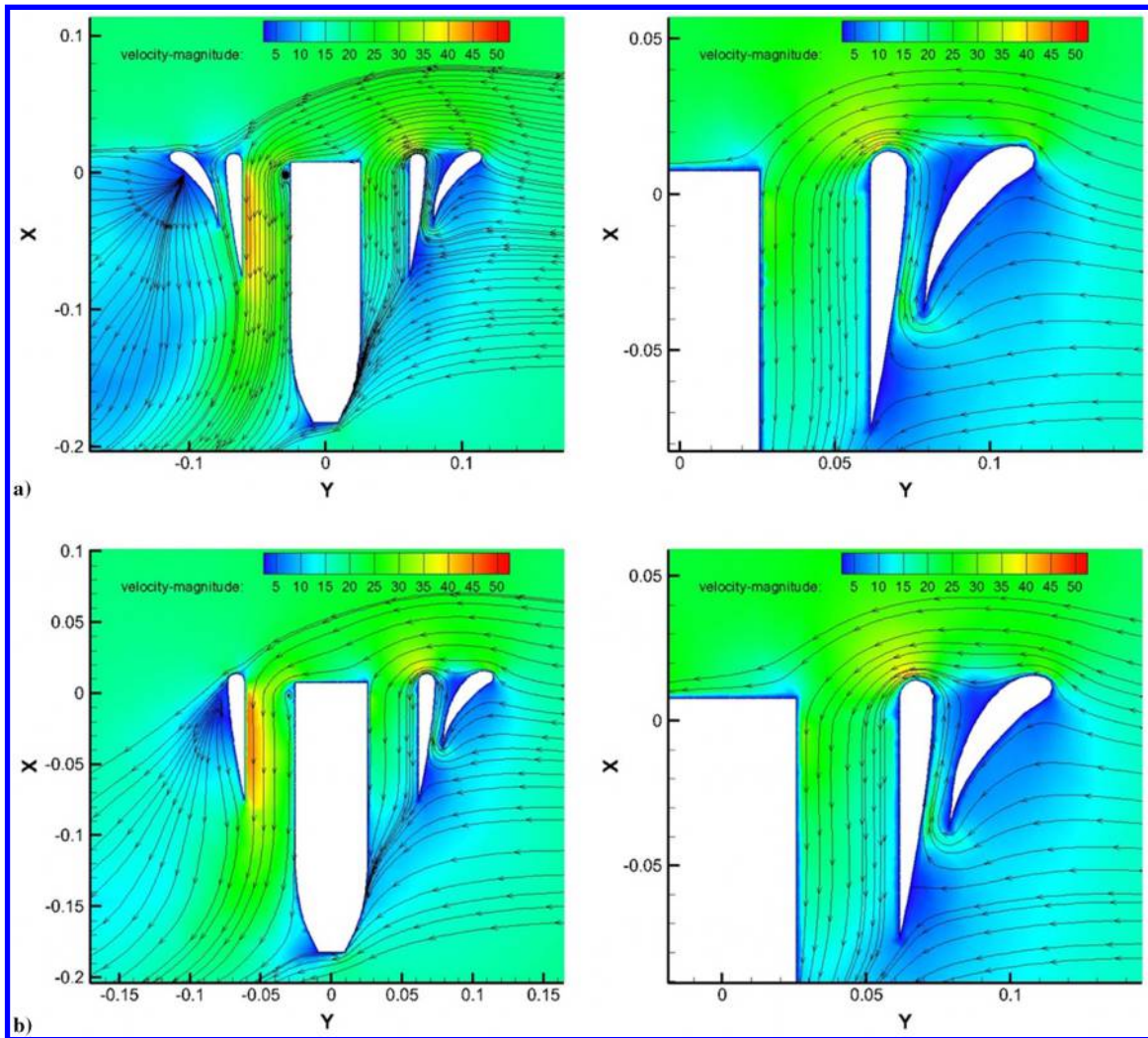
Fig. 23   a) 360° DDF (case B), and b) partial double-ducted fan (PDDF) local velocity magnitude and streamline comparison.

Figures 23a and 23b reveal the local velocity magnitudes and streamlines near the leading side of the DDF and PDDF, respectively. The inlet-lip-separation control ability of the partial treatment PDDF is highly similar to that of the DDF with a possibly heavy and bulky 360° duct. The present computations indicate that the wake of the vehicle for the PDDF is relatively smaller with a measurable increase in local momentum values, Fig. 23b. The area coverage of the low-momentum wake zones (dark blue) of the DDF (Fig. 23a) is reduced compared to that of the PDDF (Fig. 23b). A measurable reduction in the vehicle's drag coefficient results when the PDDF concept is adequately implemented in the forward flight regime.
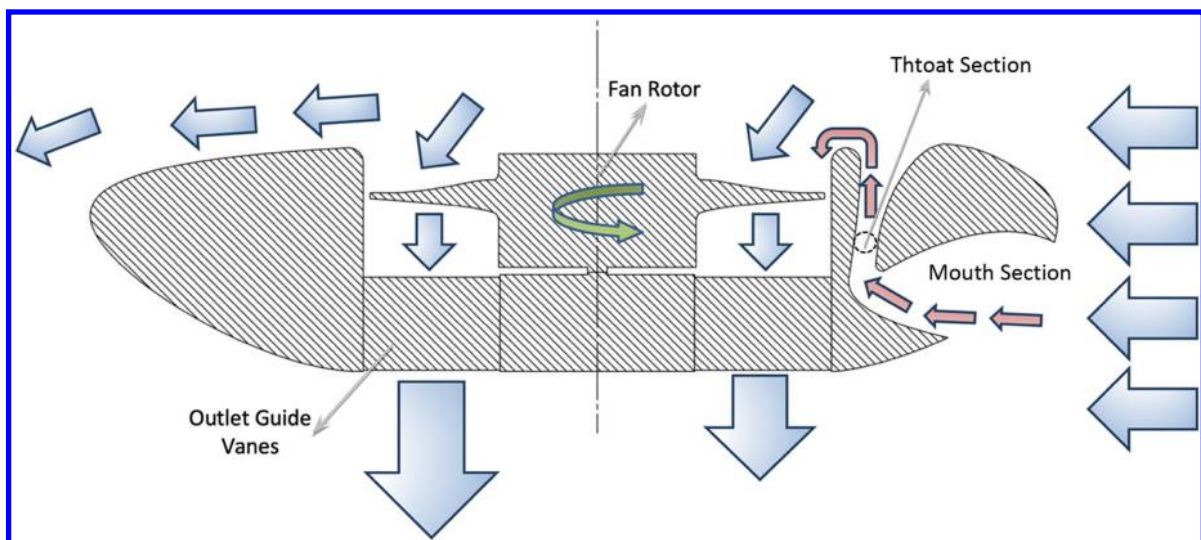

Fig. 24   Cross-sectional view of PDDF in a wing; a fan-in-wing implementation.
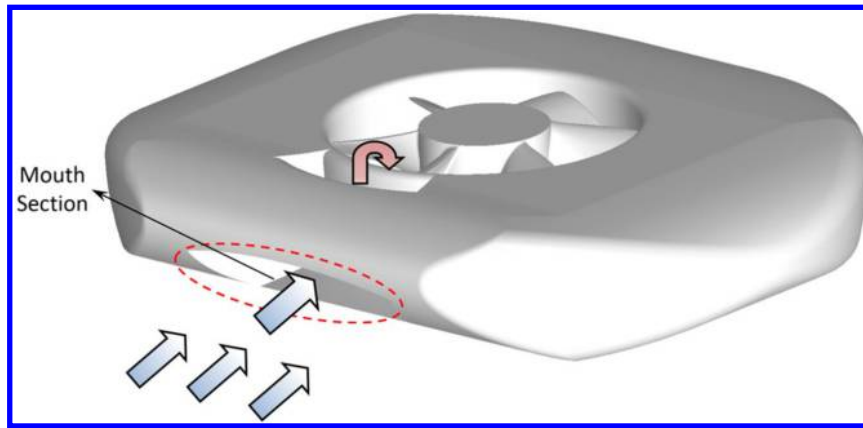
Fig. 25   Isometric view of PDDF in a wing.

B.   Fan-in-Wing Implementation of the Partial DDF (PDDF)

Figure 24 explains a fan-in-wing-type vehicle implementation of the partial DDF concept. This type of implementation fully preserves the general aerodynamic character of the PDDF. The fan-in-wing application shown in Fig. 24 is a good possibility, as far as a smooth vehicle integration of the PDDF is concerned. The avoidance of the fan's inherent inlet lip separation is achieved by embedding the partial duct into the leading-edge area of the wing or vehicle body. A three-dimensional implementation of the leading-edge mouth section can be effective in VTOL vehicles having a lifting-body-type cross section or lifting fans integrated into wing areas.

The total pressure available just in front of the mouth section drives the flow into the second duct through a throat section. Similar deceleration characteristics existing in the outer duct of a typical DDF are observed just after the throat section. The flow after the throat shown in Fig. 24 slightly decelerates and forms an upward boundary-layer flow over a convex surface. The well-attached boundary-layer flow between points C, B, A, and O is essential for lip separation control, just before it smoothly turns around the lip. Figure 20b shows the locations of C, B, A, and O. The typical lip separation of the flow turning into the rotor area can be effectively controlled using this novel concept called "PDDF embedded in a wing" during the edgewise flight of a VTOL vehicle, as shown in Fig. 25.

VIII.   Conclusions

This paper describes a new ducted-fan inlet flow conditioning concept that has an excellent potential to improve the performance and controllability of ducted-fan-based VTOL vehicles, UAVs, and fan-in-wing-type vehicles. The new (DDF) concept developed in this study deals with various apparent aerodynamic problems in ducted fans operating at an almost 90 deg angle of attack in the edgewise flight mode.

The new concept that significantly reduces the inlet lip separation in the edgewise flight zone is named double-ducted fan (DDF). The concept development effort uses a RANS-based 3-D computational flow solution explicitly developed for ducted fan flows. The present study summarizes only the most promising designs after evaluating nine different double-ducted fan geometries for a wide range of edgewise flight velocities.

The DDF concept uses a secondary stationary duct system to control inlet lip separation near the fan rotor's inlet occurring at elevated edgewise flight velocities. The DDF is effectively operational in a broad edgewise flight velocity regime.

DDFs corrective aerodynamic influence becomes more pronounced with increasing flight velocity due to its inherent flow characteristics.

Case B was the best DDF configuration designed. It has improved mass flow rate passing from the duct by 40% and has improved thrust force obtained from the ducted fan by 56.2% relative to baseline duct in edgewise flight at 20 m/s.

A "variable double-ducted fan" implementation of the DDF provides a much more effective inlet lip separation control in a broad range of horizontal flight velocities in UAVs, air vehicles, trains, buses, and marine vehicles.

The current flow control approach could also be implemented as a partial double-ducted Fan (PDDF) only near the vehicle's leading edge. The present computations indicate that the wake of the vehicle for the PDDF is relatively smaller, with a measurable increase in local momentum values. A measurable reduction in the vehicle's drag coefficient results when the PDDF concept is adequately implemented in the forward flight regime.

A fan-in-wing-type vehicle implementation of the partial DDF concept is possible. The avoidance of the fan's inherent inlet lip separation is achieved by embedding the partial duct into the leading-edge area of the wing or vehicle body.

Most axial flow fans are designed for an inlet flow with zero or minimal inlet flow distortion. The DDF concept is proven to be an effective way of dealing with inlet flow distortions occurring near the tip section of an axial flow fan rotor system operating at a high angle of attack.

Acknowledgments

References

[1] McCormick, B. W., *Aerodynamics of V/STOL Flight*, Dover, New York, 1999, p. 245.

[2] Lazareff, M., "Aerodynamics of Shrouded Propellers," *The Aerodynamics of V/STOL Aircraft*, Rhode Saint Genese, A Lecture Series jointly sponsored by AGARD and the von Karman Institute, 1968, pp. 239–289.

[3] Abrego, A. I., and Bulaga, R. W., "Performance Study of a Ducted Fan System," *American Helicopter Society (AHS) Aerodynamics, Aeroacoustic, Test and Evaluation Technical Specialist Meeting*, San Francisco, CA, Jan. 2002.

[4] Martin, P., and Tung, C., "Performance and Flowfield Measurements on a 10-Inch Ducted Rotor VTOL UAV," *60th Annual Forum of the American Helicopter Society*, Baltimore, 2004.

[5] Graf, W. E., Fleming, J., and Wing, N., "Improving Ducted Fan UAV Aerodynamics in Forward Flight," *46th AIAA Aerospace Sciences Meeting and Exhibit*, AIAA Paper 2008-0430, Reno, NV, 2008.
https://doi.org/10.2514/6.2008-430

[6] Graf, W. E., "Effects of Duct Lip Shaping and Various Control Devices on the Hover and Forward Flight Performance of Ducted Fan UAVs," Master's Thesis, Virginia Polytechnic Inst. and State Univ., Blacksburg, VA, 2005.

[7] Kriebel, A. R., and Mendenhall, M. R., "Predicted and Measured Performance of Two Full-Scale Ducted Propellers," *Cornell Aeronautical Lab (CAL)/USAAVLABS Symposium on Aerodynamic Problems Associated with V/STOL Aircraft, Vol II: Propulsion and Interference Aerodynamics*, Buffalo, New York, 1966.

[8] Mort, K. W., and Gamse, B., "A Wind Tunnel Investigation of a 7-Foot-Diameter Ducted Propeller," NASA TND-4142, 1967.

[9] Mort, K. W., and Yaggy, P. F., "Aerodynamic Characteristics of a 4-Foot-Diameter Ducted Fan Mounted on the Tip of a Semispan Wing," NASA TND-1301, 1962.

[10] Yaggy, P. F.,, and Mort, K. W., "A Wind-Tunnel Investigation of a 4-Foot-Diameter Ducted Fan Mounted on the Tip of a Semispan Wing," NASA TND-776, 1961.

[11] Lind, R., Nathman, J. K., and Gilchrist, I., "Ducted Rotor Performance Calculations and Comparisons with Experimental Data," *44th AIAA Aerospace Sciences Meeting and Exhibit*, AIAA Paper 2006-1069, Reno, Nevada, 2006.
https://doi.org/10.2514/6.2006-1069

[12] He, C., and Xin, H., "An Unsteady Ducted Fan Model for Rotorcraft Flight Simulation," *62nd American Helicopter Society Forum*, Phoenix, 2006.

[13] Chang, I. C., and Rajagopalan, R. J., "CFD Analysis for Ducted Fans with Validation," *21th AIAA Applied Aerodynamics Conference*, AIAA Paper 2003-4079, Orlando, 2003.
https://doi.org/10.2514/6.2003-4079

[14] Ahn, J., and Lee, K., "Performance Prediction and Design of a Ducted Fan System," *40th AIAA/ASME/SAE/ASEE Joint Propulsion Conference and Exhibit*, AIAA Paper 2004-4196, Fort Lauderdale, 2004.
https://doi.org/10.2514/6.2004-4196

[15] Ko, A., Ohanian, O. J., and Gelhausen, P., "Ducted Fan UAV Modeling and Simulation in Preliminary Design," *AIAA Modeling and Simulation Technologies Conference and Exhibit*, AIAA Paper 2007-6375, South Carolina, 2007.
https://doi.org/10.2514/6.2007-6375.

[16] Zhao, H. W., and Bil, C., "Aerodynamic Design and Analysis of a VTOL Ducted-Fan UAV," *26th AIAA Applied Aerodynamics Conference*, AIAA Paper 2008-7516, Honolulu, Hawaii, 2008.
https://doi.org/10.2514/6.2008-7516

[17] Ohanian, O. J., III, Gelhausen, P. A., and Inman, D. J., "Nondimensional Modeling of Ducted-Fan Aerodynamics," *Journal of Aircraft*, Vol. 49, No. 1, 2012, pp. 126–140.
https://doi.org/10.2514/1.C031389

[18] Ohanian, O. J., III, Karni, E. D., Londenberg, W. K., Gelhausen, P. A., and Inman, D. J., "Ducted-Fan Force and Moment Control via Steady and Synthetic Jets," *Journal of Aircraft*, Vol. 48, No. 2, 2012, pp. 514–526.
https://doi.org/10.2514/1.C031110

[19] Fleming, J., Jones, T., Ng, W., Gelhausen, P., and Enns, D., "Improving Control System Effectiveness for Ducted Fan VTOL UAVs Operating in Crosswinds," *2nd AIAA UAV Conference and Workshop and Exhibit*, AIAA Paper 2003-6514, San Diego, CA, 2003.
https://doi.org/10.2514/6.2003-6514

[20] Ruzicka, G. C., Strawn, R. C., and Meadowcroft, E. T., "Discrete-Blade, Navier-Stokes Computational Fluid Dynamics Analysis of Ducted- Fan Flow," *Journal of Aircraft*, Vol. 42, No. 5, 2012, pp. 1109–1117.
https://doi.org/10.2514/1.8731

[21] Gray, R. B., and Wright, T., "A Vortex Wake Model for Optimum Heavily Loaded Ducted Fans," *Journal of Aircraft*, Vol. 7, No. 2, 2012, pp. 152–158.
https://doi.org/10.2514/3.44139

[22] Wright, T., "Evaluation of the Design Parameters for Optimum Heavily Loaded Ducted Fans," *Journal of Aircraft*, Vol. 7, No. 6, 1970, pp. 512–517.

[23] Jiang, Y., Zhang, B., and Huang, T., "CFD Study of an Annular-Ducted Fan Lift System for VTOL Aircraft.," *Aerospace*, Vol. 2, No. 4, 2015, pp. 555–580.
https://doi.org/10.3390/aerospace2040555

[24] Sheng, C., and Zhao, Q., "Numerical Investigations of Fan-in-Wing Aerodynamic Performance with Active Flow Control," *Journal of Aircraft*, Vol. 54, No. 6, 2017, pp. 2317–2329.
https://doi.org/10.2514/1.C034134

[25] Hoeveler, B., Bauknecht, A., Wolf, C. C., and Janser, F., "Wind-Tunnel Study of a Wing-Embedded Lifting Fan Remaining Open in Cruise Flight," *Journal of Aircraft*, Vol. 57, No. 4, 2020, pp. 558–568.
https://doi.org/10.2514/1.C035422

[26] Yılmaz, S., Erdem, D., and Kavsaoglu, M. S., "Performance of a Ducted Propeller Designed for UAV Applications at Zero Angle of Attack Flight: An Experimental Study," *Aerospace Science and Technology*, Vol. 45, Sept. 2015, pp. 376–386.
https://doi.org/10.1016/j.ast.2015.06.005

[27] Werle, M. J., "Analytical Model for Ring-Wing Propulsor Thrust Augmentation," *Journal of Aircraft*, Vol. 57, No. 5, 2020, pp. 901–913.
https://doi.org/10.2514/1.C035922

[28] Akturk, A., Shavalikul, A., and Camci, C., "PIV Measurements and Computational Study of a 5-Inch Ducted Fan for V/STOL UAV Applications," *47th AIAA Aerospace Sciences Meeting and Exhibit*, AIAA Paper 2009-0332, Orlando, FL, 2009.
https://doi.org/10.2514/6.2009-332

[29] Akturk, A., and Camci, C., "Experimental and Computational Assessment of a Ducted-Fan Rotor Flow Model," *Journal of Aircraft*, Vol. 49, No. 3, 2012, pp. 885–897.
https://doi.org/10.2514/1.C031562

[30] Akturk, A., and Camci, C., "Tip Clearance Investigation of a Ducted Fan Used in VTOL UAVs, Part 1: Baseline Experiments and Computational Validation," *ASME Journal of Turbomachinery*, Vol. 136, No. 2, 2014, Paper 021004.
https://doi.org/10.1115/1.4023468

[31] Akturk, A., and Camci, C., "Tip Clearance Investigation of a Ducted Fan used in VTOL UAVs, Part 2: Novel Treatments via Computational Design and their Experimental Verification," *ASME Journal of Turbomachinery*, Vol. 136, No. 2, 2014, Paper 021005.
https://doi.org/10.1115/1.4023469

[32] Camci, C., Akturk, A., and Herwig, N., "Inlet Flow Separation Control via Novel Lip-Spoilers for Ducted Fan Based VTOL uninhabited aerial Vehicles," *Proceedings of the 2016 ISROMAC International Symposium on Transport Phenomenon and Dynamics of Rotating Machinery*, Honolulu, Hawaii, 2016, https://hal.archives-ouvertes.fr/hal-01887487.

[33] Akturk, A., and Camci, C., "Lip Separation and Inlet Flow Distortion Control in Ducted Fans used in VTOL Systems," *IGTI ASME International Gas Turbine Conference*, ASME Paper GT2014-26249, Dusseldorf, Germany, 2014.
https://doi.org/10.1115/GT2014-26249

[34] Camci, C., and Akturk, A., "Double-Ducted Fan," U.S. Patent Publication Number 2011 0217163 A1, 2011.

[35] Ansys Inc., *ANSYS-FLUENT v12 User's Guide*, Canonsburg, Pennsylvania, 2009.